AD/A-006 260

CHARACTERIZATION OF 2014-T651 ALUMINUM ALLOY

R. J. Reid, et al

Terra Tek, Incorporated

Prepared for:

Army Materials and Mechanics Research Center

November 1974

UNCLASSIFIED

SECURITY CLASSIFICATION OF THIS PAGE (When Data Entered)

REPORT DOCUMENTATION PAGE		READ INSTRUCTIONS BEFORE COMPLETING FORM
1. REPORT NUMBER AMMRC CTR 74-68	2. GOVT ACCESSION NO.	3. RECIPIENT'S CATALOG NUMBER AD/A-006260
4. TITLE (and Subtitle) CHARACTERIZATION OF 2014-T651 ALUMINUM ALLOY		5. TYPE OF REPORT & PERIOD COVERED Final, [redacted]
		6. PERFORMING ORG. REPORT NUMBER TR 74-35
7. AUTHOR(s) Reid, R. J. Jones, A. H. Green, S. J.		8. CONTRACT OR GRANT NUMBER(s) DAAG46-74-C-0019
9. PERFORMING ORGANIZATION NAME AND ADDRESS Terra Tek, Inc. 420 Wakara Way Salt Lake City, Utah 84108		10. PROGRAM ELEMENT, PROJECT, TASK AREA & WORK UNIT NUMBERS D/A Project: AMCMS Code: Agency Accession:
11. CONTROLLING OFFICE NAME AND ADDRESS Army Materials and Mechanics Research Center Watertown, Massachusetts 02172		12. REPORT DATE November 1974 13. NUMBER OF PAGES 54
14. MONITORING AGENCY NAME & ADDRESS(if different from Controlling Office)		15. SECURITY CLASS. (of this report) Unclassified 15a. DECLASSIFICATION/DOWNGRADING SCHEDULE

16. DISTRIBUTION STATEMENT (of this Report)

Approved for public release; distribution unlimited.

17. DISTRIBUTION STATEMENT (of the abstract entered in Block 20, if different from Report)

18. SUPPLEMENTARY NOTES

19. KEY WORDS (Continue on reverse side if necessary and identify by block number)

Aluminum
Stress-strain
Bearing tests
Biaxial stresses
Yield
Fracture
Strain-rate

20. ABSTRACT (Continue on reverse side if necessary and identify by block number)

The mechanical properties of 2014-T651 aluminum alloy were determined at room temperature under various strain rates and stress states. Uniaxial tension and compression tests were performed at strain rates ranging from 10^{-5} to 10^{3} sec^{-1}. Biaxial stress tests were conducted at rates of 10^{-4} and 1 sec^{-1}. The biaxial stress states were obtained with thin walled tubular specimens loaded with a combination of axial tension/compression, internal pressure, torsion and external pressure with any two loads superimposed for any given test.

DD FORM 1 JAN 73 1473 EDITION OF 1 NOV 65 IS OBSOLETE

UNCLASSIFIED

SECURITY CLASSIFICATION OF THIS PAGE (When Data Entered)

20. The experimentally observed yield agrees with the von Mises yield condition. Strain to failure exhibited a high degree of anisotropy; ductility being minimum in the thickness direction. Fracture toughness and pin bearing strength properties were also determined.

TABLE OF CONTENTS

LIST OF ILLUSTRATIONS

LIST OF TABLES

INTRODUCTION

The AMMRC sponsored program is to provide mechanical characterization data for candidate anti-ballistic missile structural materials for use in design studies and vulnerability analysis. Various tests have been conducted on 2014-T651 aluminum alloy in order to determine the mechanical properties as a function of strain rate under both uniaxial and biaxial stress conditions. In addition, the fracture toughness and pin bearing strength of the material were determined according to standard A.S.T.M. methods.

The uniaxial tension and compression tests were run at rates from 10^{-5} to 10^{3} sec^{-1} while the biaxial tests were run at rates from 10^{-4} sec^{-1} to 1 sec^{-1}. The biaxial tests were performed in the tension-tension, tension-compression (compression-shear) and compression-tension (tension-shear) stress quadrants, with the tests run on tubular specimens using a combination of axial tension or compression, internal pressure, external pressure and torsion. These combined stress tests were performed at constant stress ratios to failure. The fracture toughness was determined at two different loading rates on two specimen configurations. ASTM compact fracture toughness specimens configurations were used as opposed to the ASTM bend specimen. Two different edge distance ratios and three plate thicknesses were tested to determine the pin bearing strength of the material.

The majority of the tests, including fracture toughness and pin bearing strength, were run on a servo-controlled hydraulic test machine designed and built by Terra Tek. This machine covered rates from 10^{-5} to 10 sec^{-1} while the higher rate uniaxial tests were run on a split Hopkinson facility.

MATERIAL DESCRIPTION

Kaiser 2014-T651 (AMS4014) aluminum alloy was obtained from the Army Materials and Mechanics Research Center in the form of three 2 inch thick rolled plates. A sample of the material was subjected to metallurgical examination to determine the in-plate directions parallel and transverse to the rolling direction. At a magnification of 53X, photomicrographs reveal flattened and elongated grains such that their length in the direction of rolling, width and thickness dimensions are roughly in the ratio of 6:5:1. The length of a grain is about 1-1/4 to 1-1/2 millimeters. The photomicrographs and their orientations with respect to the plate directions are shown in Figure 1. One inch on the photos corresponds to 0.5 millimeter in the material.

The majority of the specimens tested in this phase of the work were taken with their axis in the rolling direction of the plate (i.e., major axis parallel to the rolling direction). Additional uniaxial stress tests were, however, performed with the specimen major axis in the plate thickness and width directions.

TEST METHODS

Since the test program required such a wide range of strain rates and test types a detailed description of the equipment and procedures used to perform the program appears to be appropriate. This section will deal with that description.

Medium Strain Rate Machine

As was pointed out earlier all but the highest rate uniaxial tests were performed on a high speed, servo controlled, hydraulically actuated test machine. A photograph of the machine and accompanying controls is shown in Figure 2.

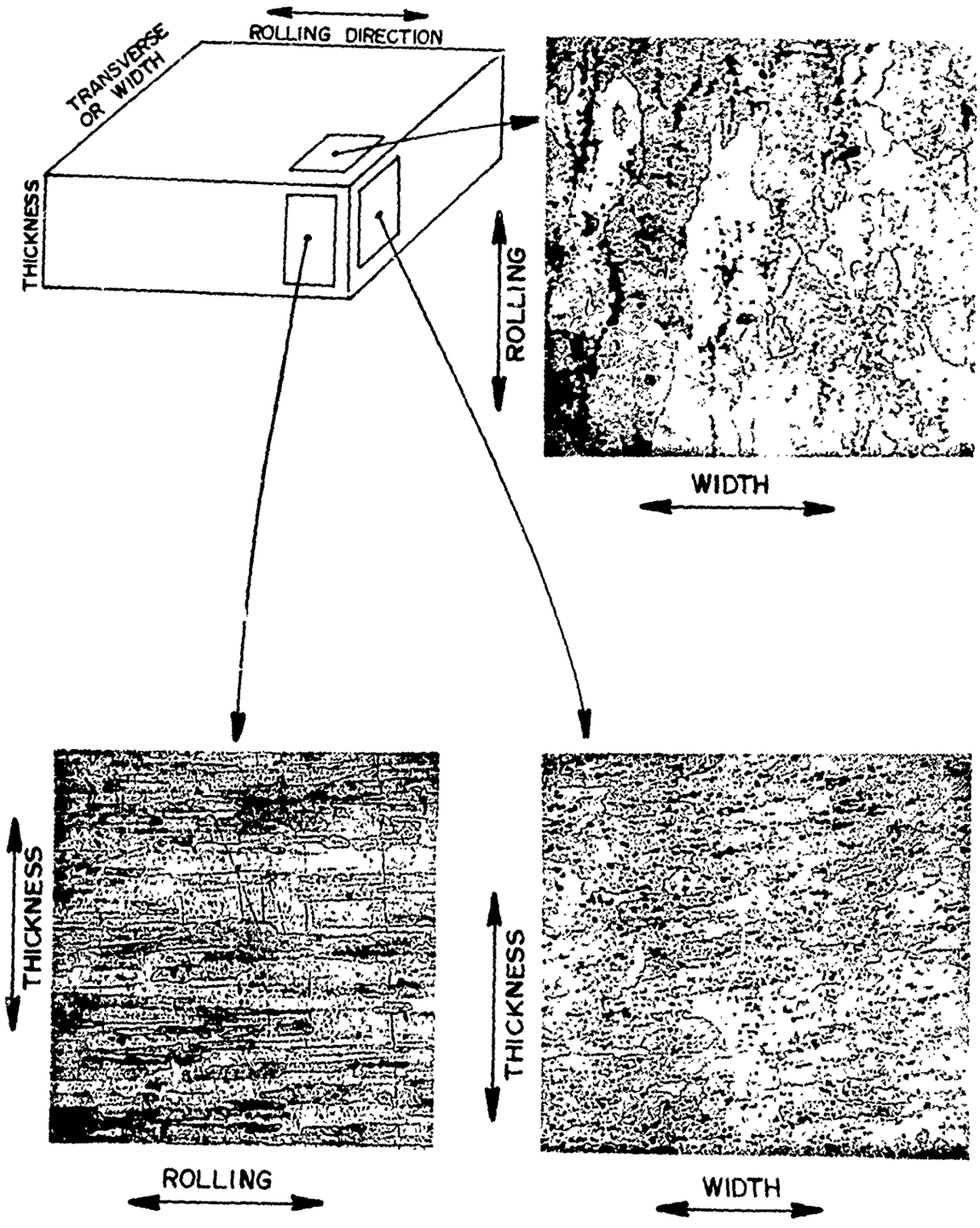

Figure 1. Photomicrographs of 2014-T651 Aluminum Plate

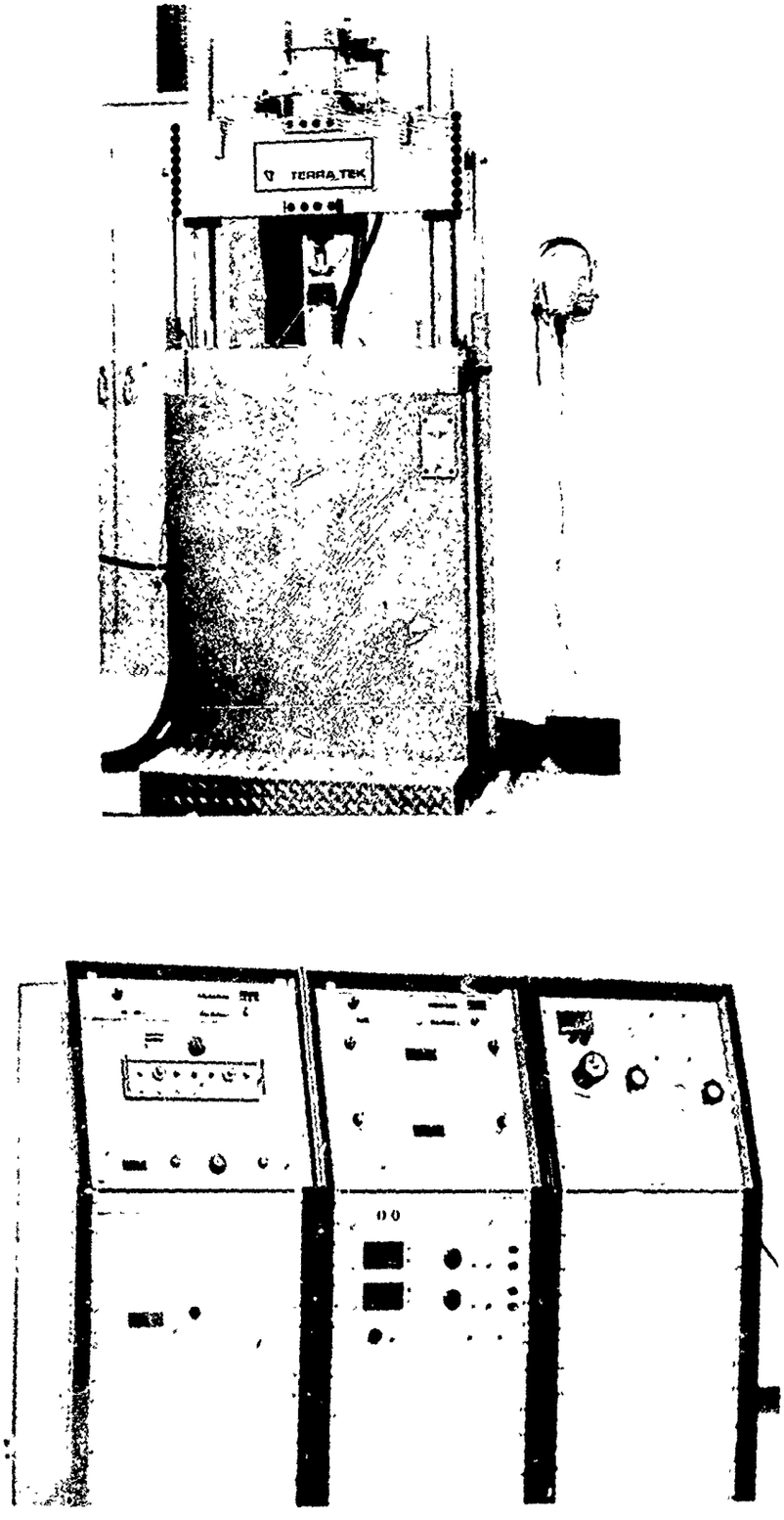

Figure 2. Axial/Biaxial Medium Strain Rate Machine.

Axial Hydraulic Actuators

The machine consists of a loading frame having two smooth columns with two adjustable platens. The lower platen normally remains fixed with the upper platen adjusted to various heights with the help of two attached hydraulic lift cylinders. Attached to the lower platen is a 50,000 pound 6 inch stroke linear actuator designed especially for fatigue (capable of 20 Hz). This actuator is controlled with a 15 gpm servo valve which allows strain rates of 10^{-6} to 1 sec^{-1} to be achieved.

In addition a 50 gpm 4-way solenoid operated valve is also mounted on the back of the actuator using a flow-control subplate manifold to vary the flow for open-loop operation. This valve allows the highest strain rates attainable hydraulically to be reached (10 sec^{-1}). Accumulators are used to supply the excess flow needed for these high rate tests.

Hydraulic Torsional Actuator

Attached to the linear actuator is a 30,000 in-lb 270° rotary actuator also controlled with a 15 gpm servo valve. A zero backlash coupling is used to attach this actuator to the bottom of the linear actuator; the rotary actuator is naturally removed during higher rate linear tests to reduce the moving mass. Both actuators are supplied by a 100 h.p. 50 gpm hydraulic power supply.

Axial Gas Actuator

For the intermediate rate tests (1 to 10^2 sec^{-1}) a high pressure gas actuator is attached to the upper platen. This actuator is operated by charging a large reservoir in back of the piston, and a small reservoir in front of the piston to equal pressure. The piston moves forward when the small reservoir is exhausted by flow through an orifice. Exhaust of the small reservoir is initiated through the opening of a fast acting solenoid valve

mounted downstream of the orifice. Piston velocity, and hence rate of loading, is controlled by the pressure of the working gas, the orifice size, and, to some extent, the specimen. Design of this actuator is similar to the one used by Green, et.al.(1).

Pressure Actuators

Internal and external pressure for the biaxial tests is supplied by a 20,000 psi intensifier shown in Figure 3. This intensifier is also servo-controlled and hydraulically actuated. The hydraulic actuator drives the piston into the high pressure vessel causing a change in volume of the pressurized fluid. Since the system is closed, this change in volume produces a change in pressure which is sensed by a pressure transducer. The pressurization rate can be controlled using the output of the pressure transducer. This type of control is used to control hoop strain rate under biaxial conditions.

Machine Controls

Controls for the medium strain rate machine and pressure intensifier are conveniently located in a three bay console. This console houses servo controllers for each actuator, including the intensifier, which are each capable of three feedback modes (displacement, strain, load). The servo controllers allow independent selection of the feedback mode with zero drift. Also located in the console are three digital ramp generators for rate control. An Exact Function Generator and cycle counter is used to command cyclic fatigue and keep track of the number of cycles respectively.

One bay of the console houses the pneumatic controls for the gas actuated fast acting system. The main body of the controls is made up of a digital pressure meter and pressure regulator to monitor and control the charge pressure. Micro switches activate the fast acting solenoid valves.

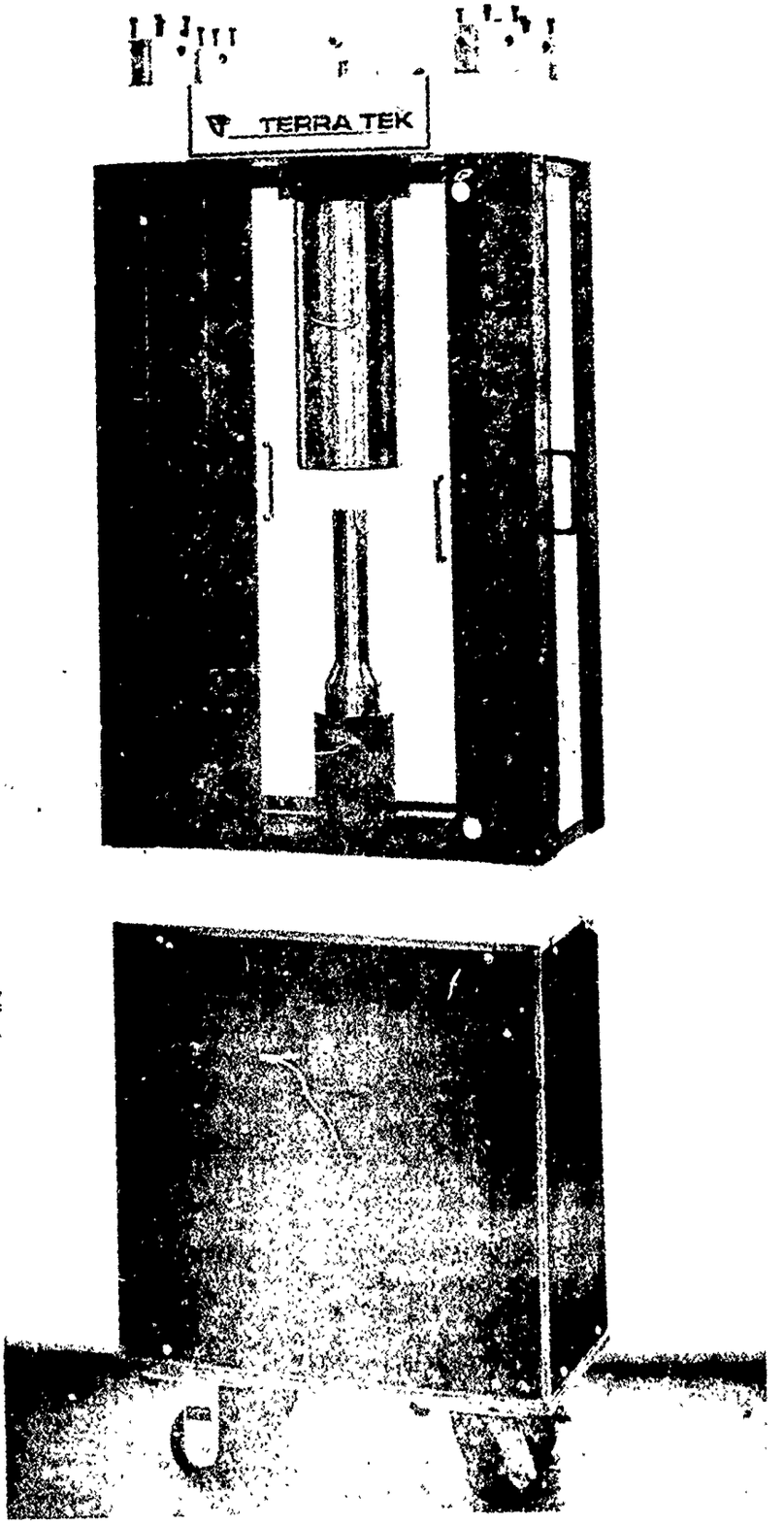

Figure 3. Pressure Intensifier.

Split Hopkinson Bar

The high rate uniaxial tension and compression tests were performed on the split Hopkinson's bar system shown in Figure 4. Depending on the bar configuration and sample properties the accessible strain rate range is from 100 to 10^4 sec^{-1}. A complete description of this apparatus is compiled elsewhere. (2,3)

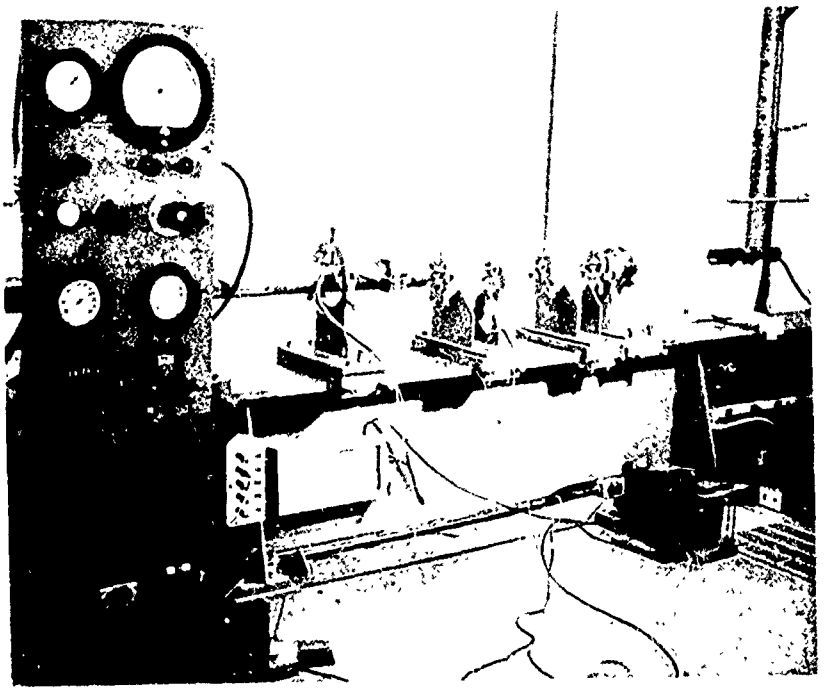

Figure 4. Split Hopkinson Bar Test Facility.

Uniaxial Tension/Compression

Uniaxial tension and compression samples were machined according to Figure 5. As indicated earlier in the text, the majority of the samples were prepared with their major axis parallel to the rolling direction of the plate. After machining, the dimensions of each sample were checked to be within the desired tolerances, the measured values were recorded to the nearest .001 inches. These values were compared to measurements taken after testing in order to check the ductility of any particular sample.

Due to the small physical size of the samples, electrical resistance strain gages were used to monitor the strain as opposed to an external strain transducer. Gages were applied using Micro-Measurements M-Bond 610 adhesive, oven cured at 350^{o}F. Micro-Measurements type EA-06-062AQ-350 gage was applied to the compressive samples while a type EA-06-031DE-120 gage was used on the tensile samples. Tests were run using two axial gages in order to assure alignment of the system. 10,000 lb. and 1,000 lb. axial force load cells were used to monitor the force on the compressive and tensile specimens respectively. Both load cells were calibrated and found to be linear to within .15% of full scale.

For the lower rate tests, strain feedback was used to drive the servo system. This allowed the strain rate to remain constant through both the elastic and plastic regions of the tests. Figure 6A is a typical test record for these tests. The higher rate tests, including the Hopkinson bar tests were run open loop, therefore, rates cited for these tests are given as an average plastic strain rate. Figure 6B is an example record for this type of test.

Data acquisition was accomplished through the system shown schematically in Figure 7. Transducers (load cell, strain gages, etc.) located at the

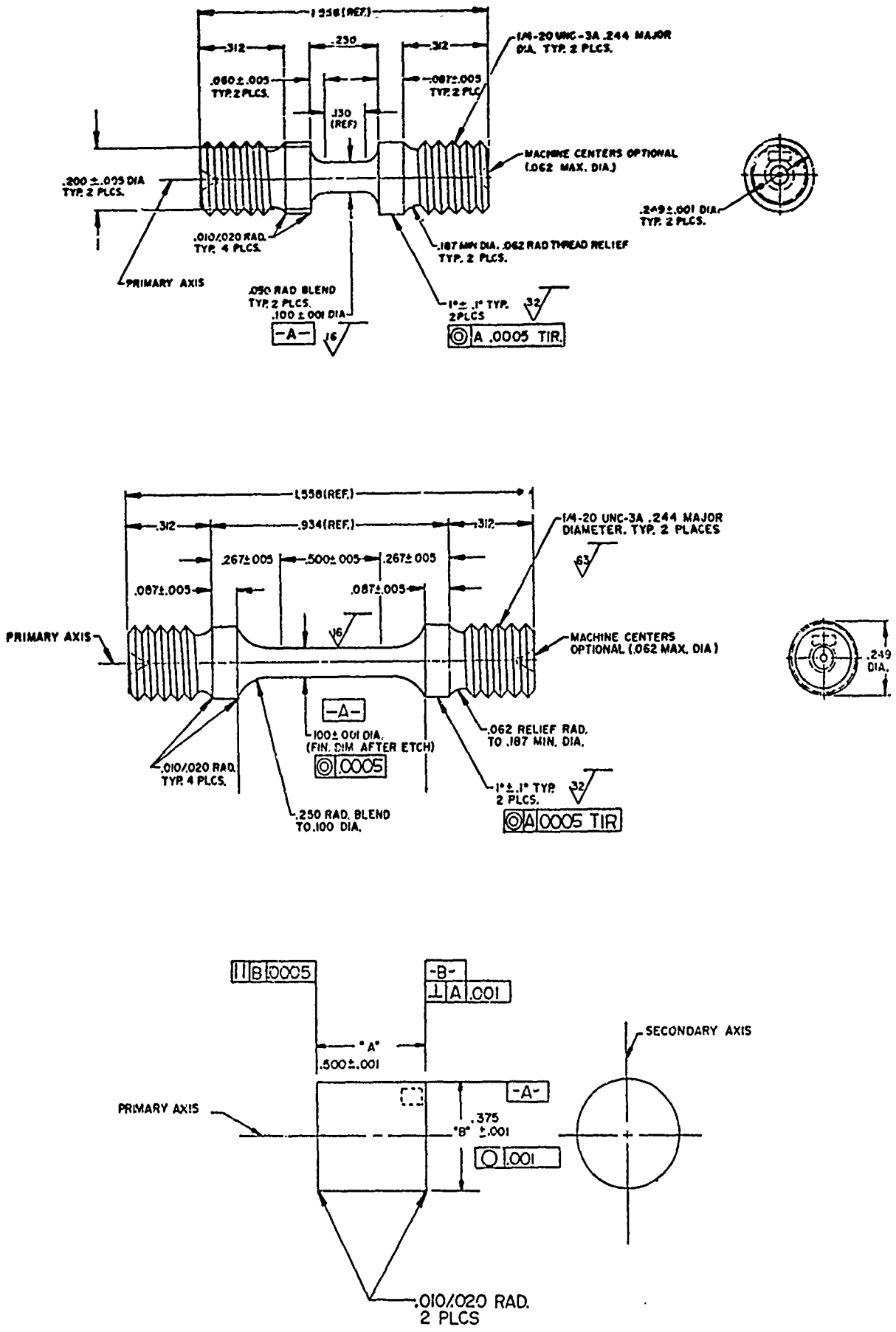

Figure 5. Uniaxial Tension and Compression Specimens

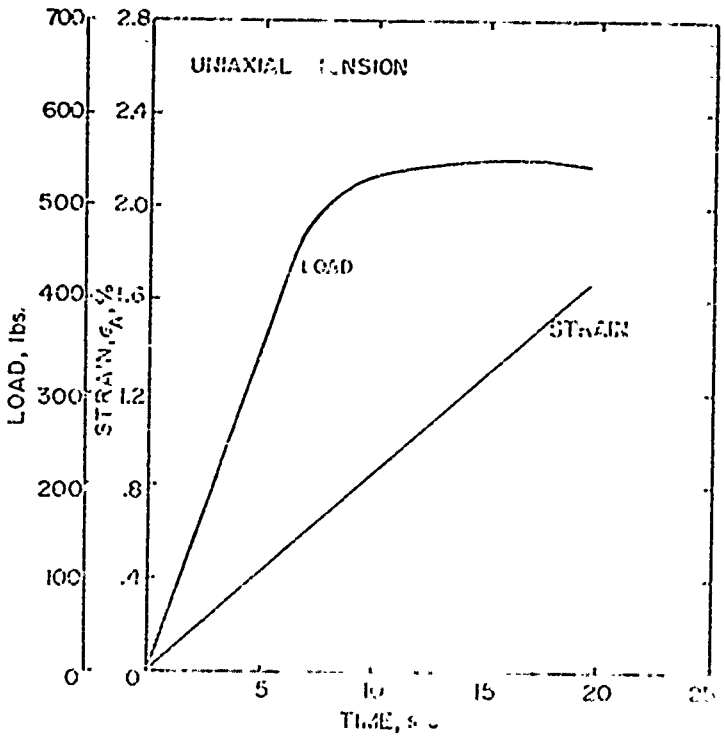

6A. Constant Strain Rate

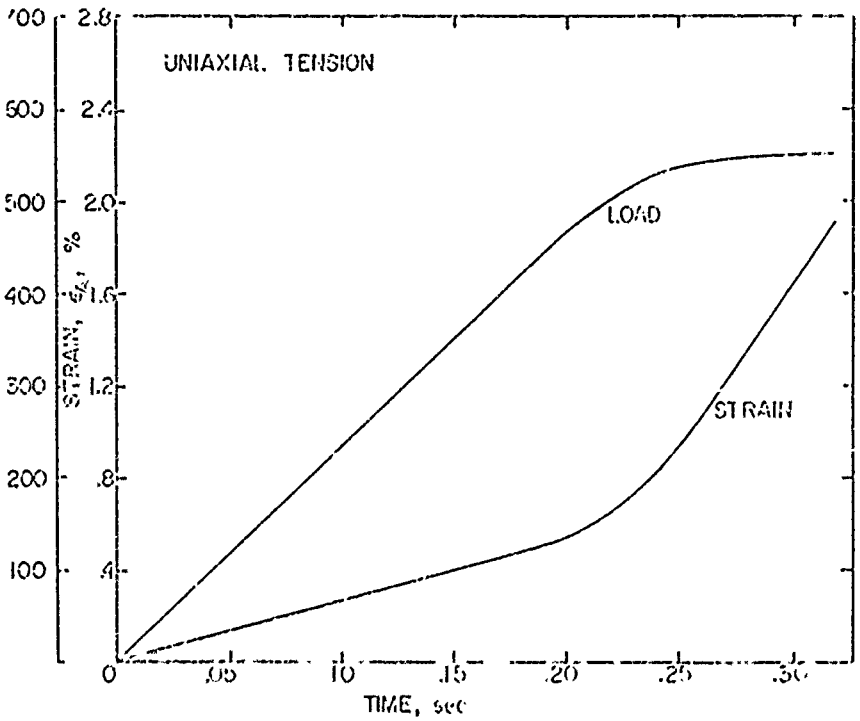

6B. Open Loop Strain Rate

Figure 6. Example Test Records for Uniaxial Stress Tests

machine were fed into a bridge completion unit, which supplied the necessary excitation voltages and resistance offset to complete standard Wheatstone bridges. The output signal from the bridge was then amplified by a type 122 D.C. Neff Amplifier with the signal recorded by one of three systems: an X-Y recorder, an oscilloscope, or with a Digital PDP Lab 11 computer. For the slower uniaxial tests a X-Y-Y' Hewlett Packard Model 7046A recorder was used. An oscilloscope was employed for the high rate tests. Tests were plotted as stress and strain -vs- time which facilitated calculation of the strain rate and the stress-strain curves.

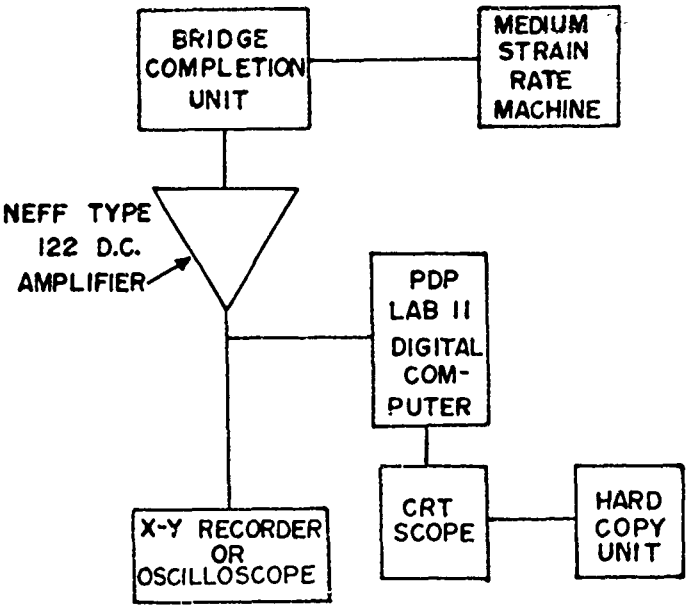

Figure 7. Schematic of Data Acquisition System

Biaxial Tests

Biaxial tests were performed on the tubular specimens shown in Figures 8 and 9. Axial tension and internal pressure tests were performed on the configuration seen in Figure 8 while axial compression, torsion and external pressure tests were performed on specimens shown in Figure 9. The method of gripping these specimens is shown in Figure 10. A threaded collar containing eight bolt holes is threaded on to the specimen leaving approximately

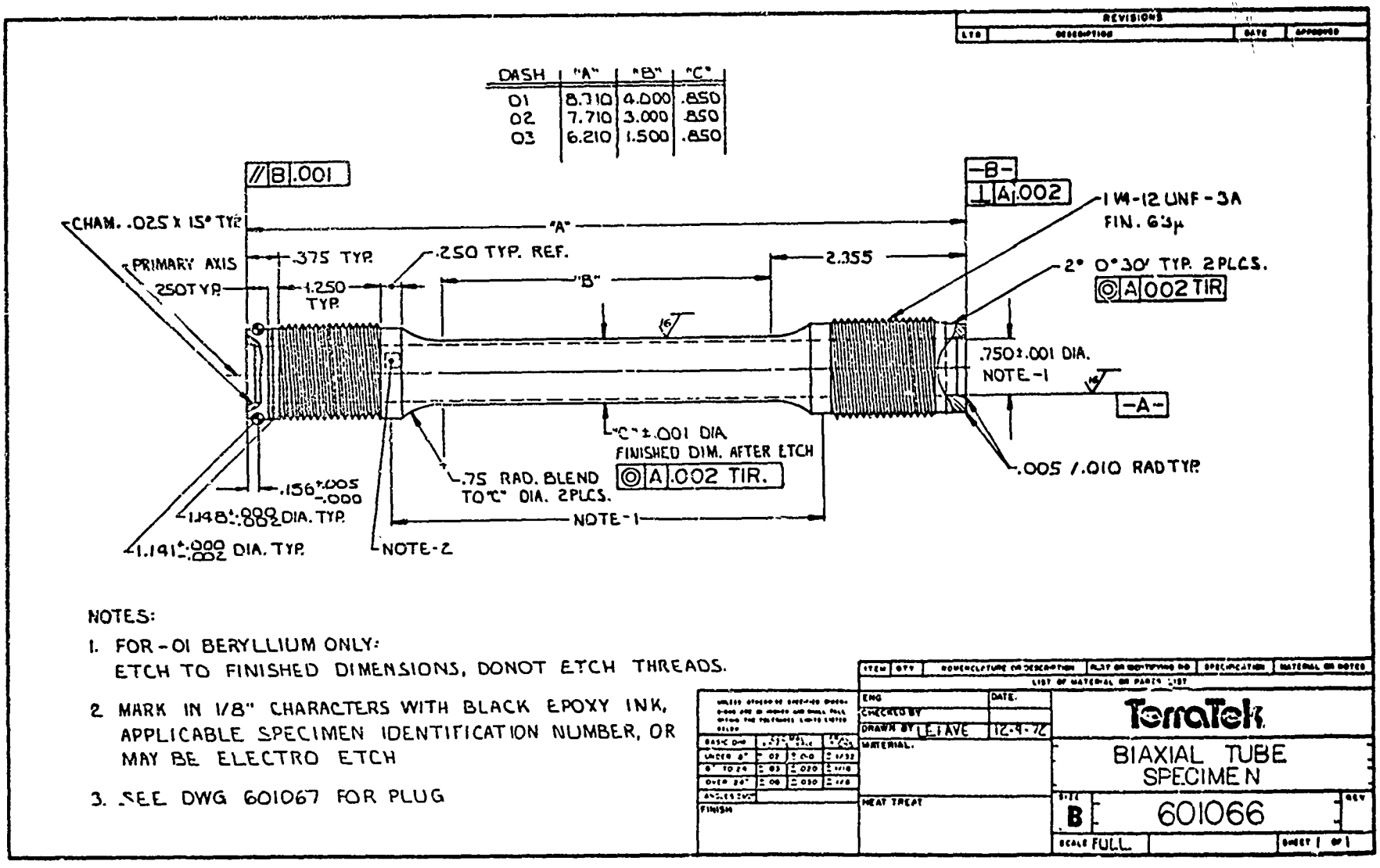

Figure 8. Tube Specimen Configuration for Axial Tension and Internal Pressure Tests.

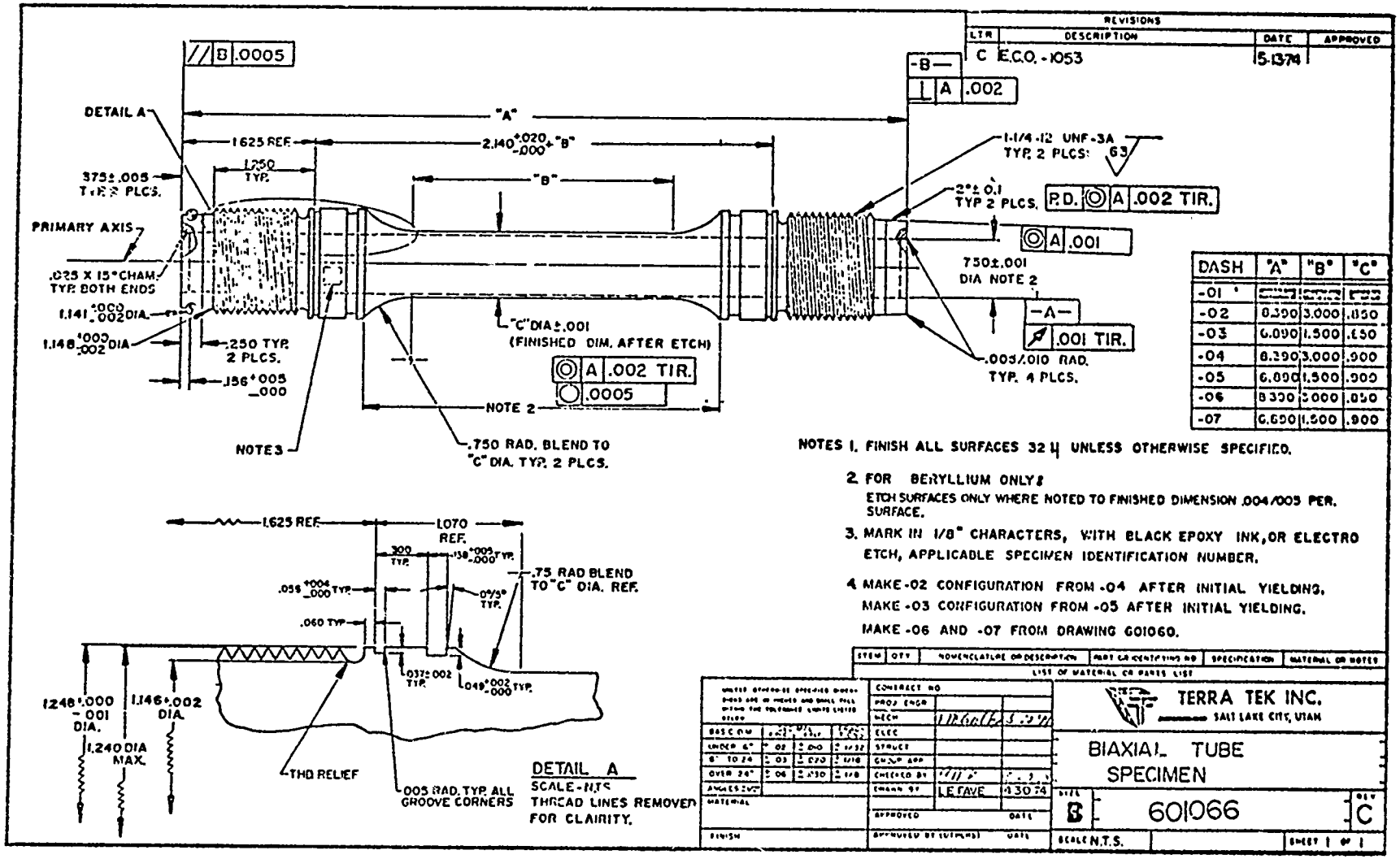

Figure 9. Tube Specimen Configuration for External Pressure, Torsion, and Axial Compression Tests.

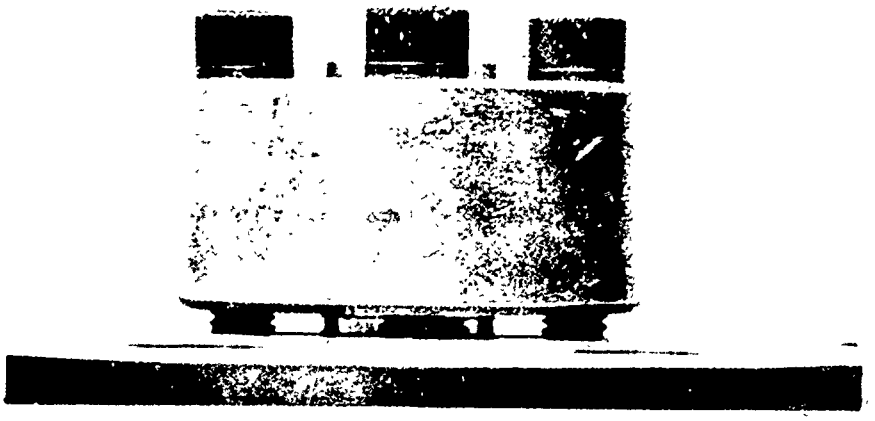

Figure 10. Biaxial Grip

1/4 inch of the specimen exposed. The taper on this exposed end allows initial alignment of the sample with respect to the loading frame. Bolts are then inserted through the collar and torqued to 150 in-lbs per bolt while maintaining alignment. This torque transposes a compressive load to the tapered end of the samples which was calculated and found to be sufficient to maintain zero slippage under a torsional load.

Torque and axial force were monitored using a 20,000 in-lb · 50,000 lb Lebow Model 6468 torque-thrust cell, linear to within .15 percent of rated capacity, with zero crosstalk between thrust and torque. A 10,000 PSI diaphragm pressure transducer, linear to .1 percent, sensed the pressure during internal and external pressurization.

For biaxial stress tests, micromeasurements type WA-06-12WR-350 strain-

gage rosettes were used to monitor the strains in three directions on the tube surface. From these three strain measurements, the principal strain magnitudes can be calculated. Two strain-gage rosettes were applied to each tubular specimen in order to check bending and any anisotropic behavior of the material. Two additional axial gages as well as the strain gage rosettes were monitored during the tightening process in order to assure that no bending moment was induced through over-tightening one side of the grip. This procedure worked very well; the two rosettes recording nearly identical strains during any particular test.

Strain gages and transducer signals were recorded using the same system described in the uniaxial tension/compression section. The one main difference being that the digital computer recorded, stored and reduced the data. The computer biaxial data acquisition routine, using BASIC computer language, could handle up to ten data channel rates for up to .1 sec^{-1} (sampling at 3 KHz). This routine also calculated the stresses from the forces and the principal strains from the strain gage data. This information was then plotted on a CRT scope from which a hard copy was obtained.

Fracture Toughness

Standard ASTM compact tension fracture toughness specimens were machined according to Figure 11. This particular geometry conforms to ASTM standards in order to give a valid fracture toughness value. The grips used for the fracture toughness test are shown in Figure 12.

The specimens were first precracked by fatigue at approximately 10 Hz using the lower linear actuator commanded by the Exact Function Generator. The fatigue process was performed under displacement control which allowed for the stress intensity at the crack tip to naturally decay off as the crack progressed. The fatigue crack length was monitored optically and the fatigue process stopped when the length of the fatigue crack exceeded .05 inches.

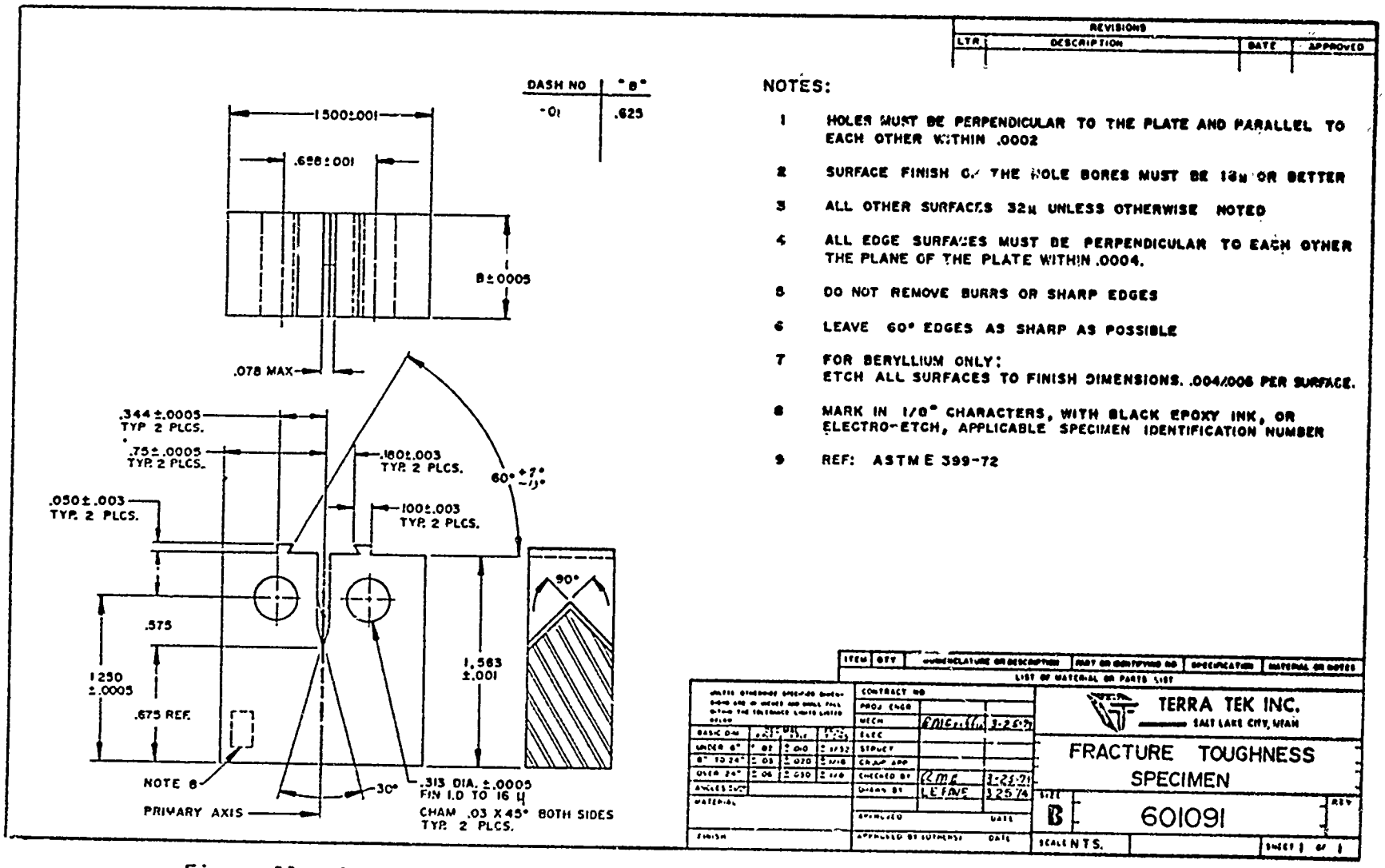

Figure 11. Specimen Configuration for Fracture Toughness Tests.

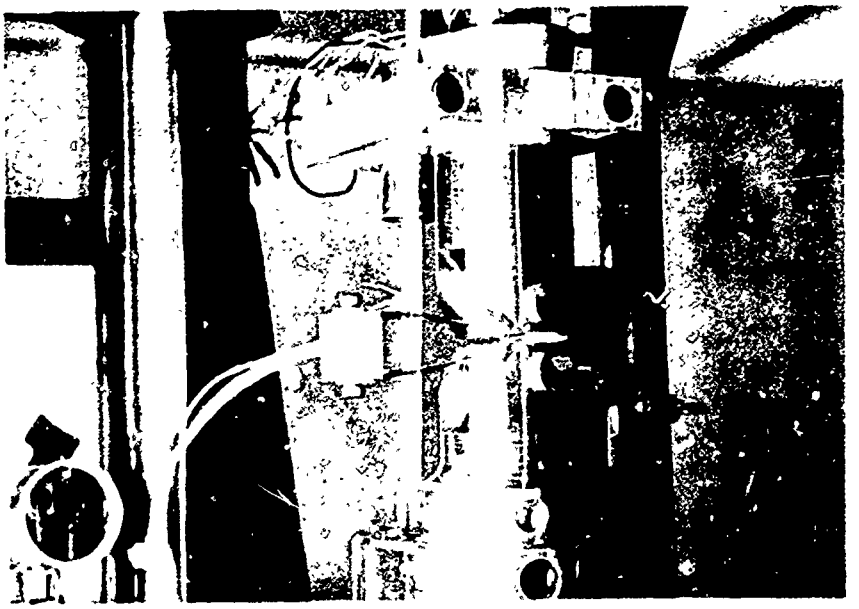

Figure 12. Fracture Toughness Grips

In the subsequent pull test the load was plotted against crack opening as measured with the clip gage attached to the notched portion of the specimen. Gage calibration was linear to within .0001 inches through .25 inches displacement.

Pin Bearing Strength

Pin-type bearing strength tests were performed according to ASTM standard E-238. The specimens were machined according to Figure 13. As can be seen from the figure, various distance ratios along with various plate thicknesses were tested. The gripping arrangement, shown in Figure 14, was used to perform this particular test. This design allowed for a miniature LVDT to be positioned above the specimen to monitor pinhole elongation.

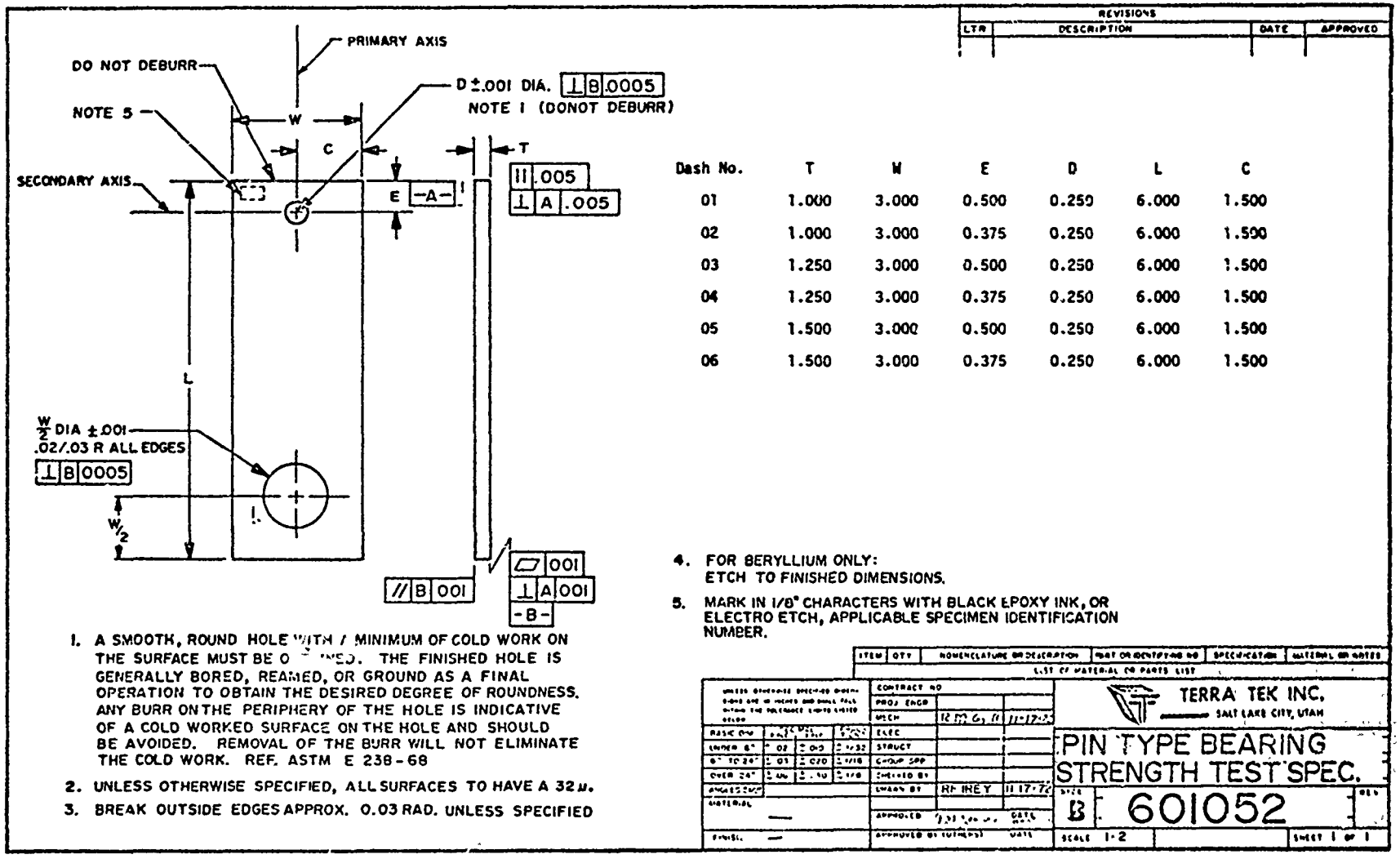

Figure 13. Pin Bearing Strength Specimen Configuration.

Figure 14. Grip Arrangement for Pin Bearing Strength Tests

A load -vs- displacement record was plotted on the X-Y recorder from which the pin-bearing strength was determined.

EXPERIMENTAL RESULTS

Ultrasonic Investigation

A 1.5 inch cube of 2014-T651 aluminum alloy was subjected to ultrasonic analysis. By exact measurement of the transit time required to pass a sound wave through the material the Young's modulus of the material can be calculated. Results of this investigation are shown in Table I.

The technique used to obtain the ultrasonic data is a through-transmission system shown schematically in Figure 15. The main advantage of this technique is the high accuracy with which the transit time of the sound wave through the specimen can be measured. The signal through the specimen is viewed on the oscilloscope, alternately with the signal from the variable frequency synthesizer after it has passed through a shaper. The shape of the latter is adjusted for an exact match of the first arrival of the wave through the specimen. The pulse that excites the transmitting transducer is next viewed and its shape matched to that of the comparison wave. Once this is done, the frequency of the synthesizer is adjusted for an exact number of cycles which, when divided by the frequency, is the transit time through the specimen. A more detailed description of the technique is available in Reference 4.

TABLE I.

ULTRASONIC VELOCITIES

SPECIMEN ORIENTATION	LONGITUDINAL VELOCITY (ft/sec)	SHEAR VELOCITY (ft/sec)	YOUNG'S MODULUS (psi)
rolling	20670	10,170	10.5×10^6
width	20640	10,100	10.6×10^6
thickness	20670	10,200	10.3×10^6
	Density = 175.62 lbs/ft^3 ≡ 2.81 gm/cm^3		

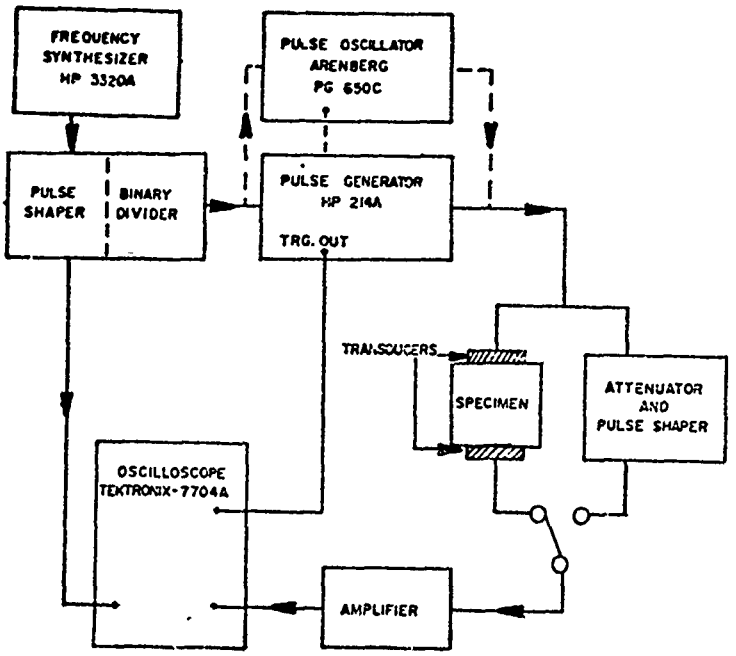

Figure 15. Schematic of the Ultrasonic "Through Transmission" System.

Uniaxial Tension/Compression

Tests performed under uniaxial stress states are listed in Table II. Uniaxial compression results for strain rates from 10^{-5} to 10 sec^{-1} are shown in Figure 16 for specimens with axes in the rolling direction. The dashed line in Figure 16 representing the true stress-strain response differs little from the engineering stress-strain curves in the region shown due to the smallness of the axial strain. Compression test results for the split-Hopkinson bar (see Reference 2 for data analysis) are shown in Figure 17 with the slower rate data superimposed. Clearly, a single curve represents all data within experimental error ($\sim$ 3%) for all strain rates.

TABLE II. UNIAXIAL STRESS TESTS PERFORMED

NUMBER OF TESTS	TENSION(T) OR COMPRESSION(C)	~ STRAIN RATE IN/IN/SEC	SPECIMEN ORIENTATION ROLLING/WIDTH/ THICKNESS	REDUCTION IN AREA %	AXIAL ELONGATION %
1	C	10^{-5}	R	-	-
2	C	10^{-4}	R	-	-
2	C	10^{-3}	R	-	-
2	C	10^{-2}	R	-	-
1	C	10^{-1}	R	-	-
2	C	1	R	-	-
1	C	10	R	-	-
2	C	1000	R	-	-
1	T	10^{-5}	R	~ 17	~ 5
2	T	10^{-4}	R	-	-
4	T	10^{-3}	R	15±3	4-6
2	T	10^{-2}	R	-	-
1	T	10^{-1}	R	-	-
1	T	1	R	~ 15	~ 5
2	T	1000	R	-	-
3	T	10^{-3}	W	15±3	~ 5
3	T	10^{-3}	T	-	~ 2.5

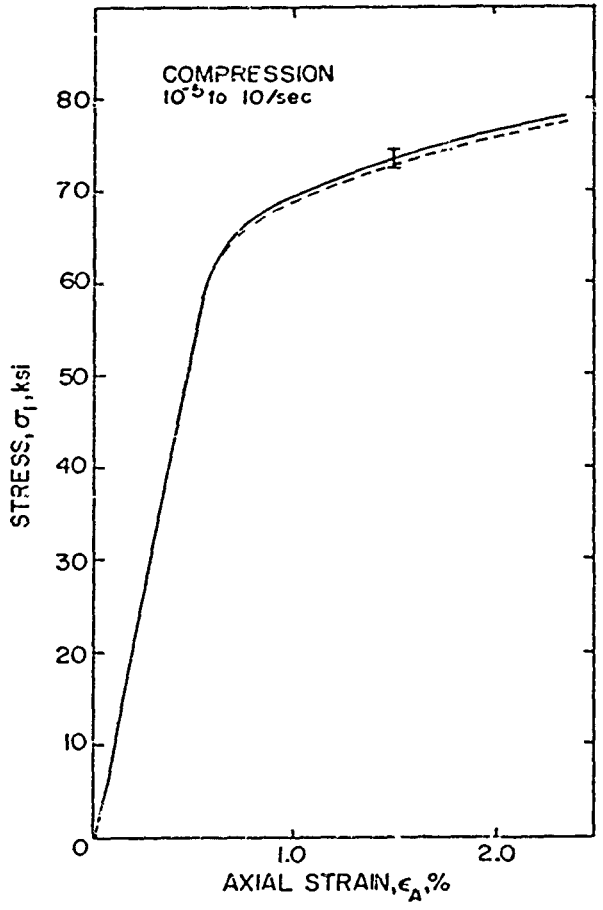

Figure 16. Stress-Strain for Uniaxial Compression.

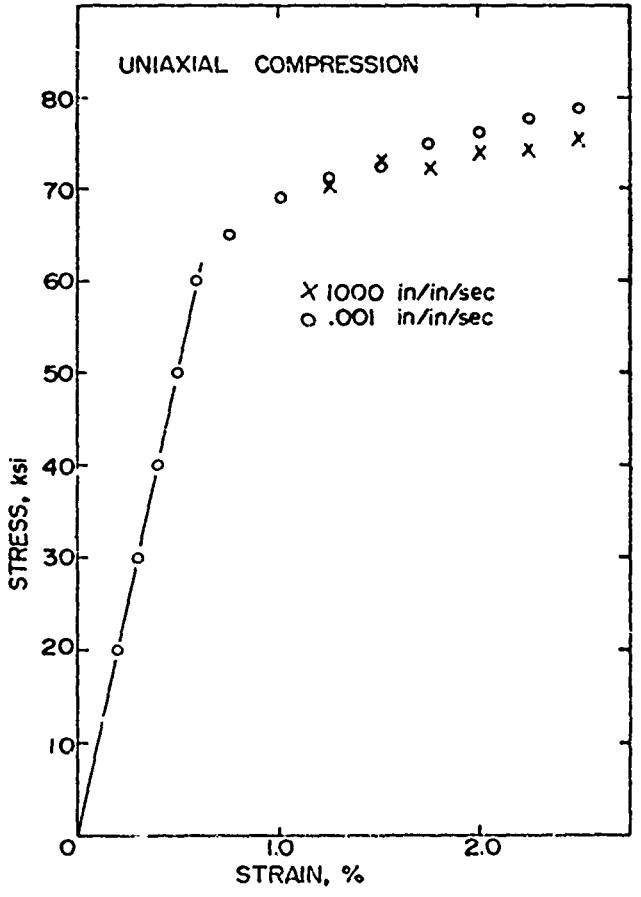

Figure 17. Stress-Strain for High Rate Uniaxial Compression.

Results for uniaxial tension tests performed in the rolling direction of the plates are seen in Figures 18 through 21. Figure 18 is the engineering stress-strain response for the tensile specimens with 0.5" gage length for strain rates from 10^{-5} to 10 sec^{-1}. Figure 19 is the response for the 0.13" gage length samples over the same strain rate range. Figure 20 combines Figures 18 and 19 indicating that the material is not strain rate sensitive and that the small specimen provides representative properties. Figure 21 represents the data observed with a split-Hopkinson bar compared directly with data taken at 10^{-3} sec^{-1}. Again, agreement is within experimental error, indicating no strain rate sensitivity to the highest strain rates tested. All tension test results show little work hardening.

Elastic modulus for the material (slope of the elastic portion of the test) is 10.4 ± 0.2 x 10^6 psi for both compression and tension. This value agrees well with the ultrasonic data and previously published data (5). Yield stress is found to be 67 ± 2 ksi for both uniaxial compression and tension. Also, uniaxial tension tests performed on specimens aligned to the thickness and width of the plate, produced elastic modulus and yield stress within the scatter band of Figure 18.

Total axial elongation to failure defined as:

$$\underset{\text{(Ductility)}}{\text{Elongation}} = \frac{L_f - L_o}{L_o}$$

where:

L_f = final gage length

L_o = initial gage length

was measured for each specimen. At failure the elongation was approximately

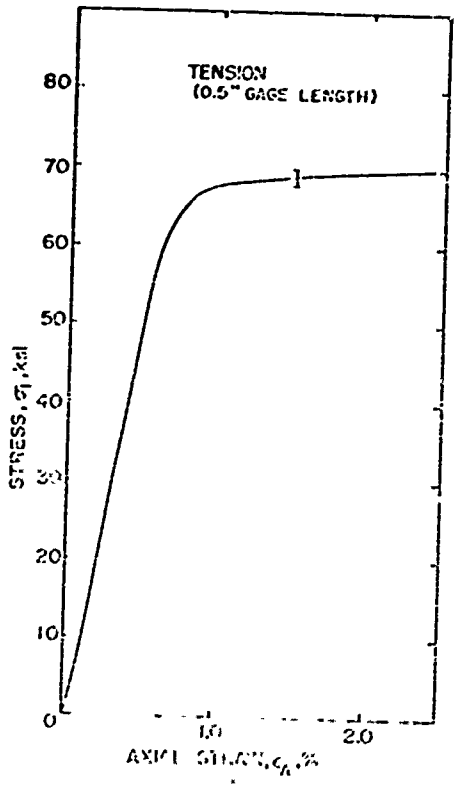

Figure 18. Stress-Strain for Uniaxial Tension (0.5" gage length)

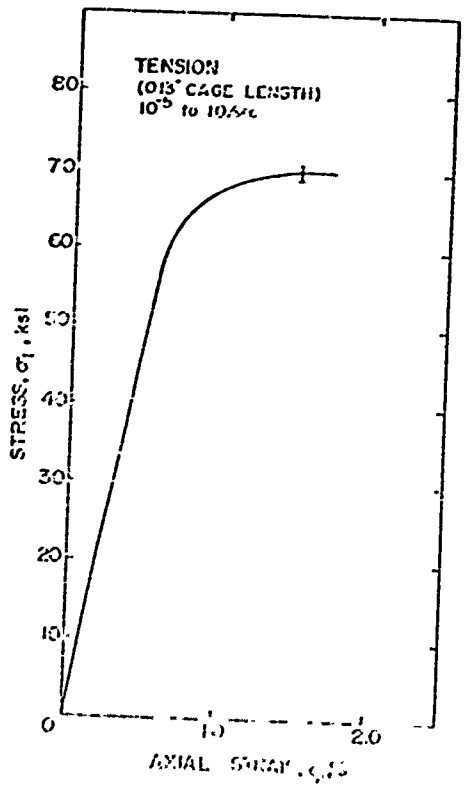

Figure 19. Stress-Strain for Uniaxial Tension (0.13" gage length)

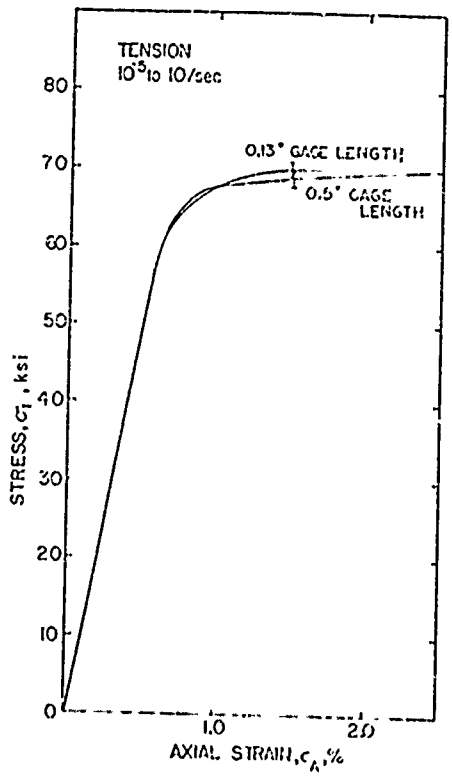

Figure 20. Stress-Strain for Uniaxial Tension (0.5 and 0.23" gage length)

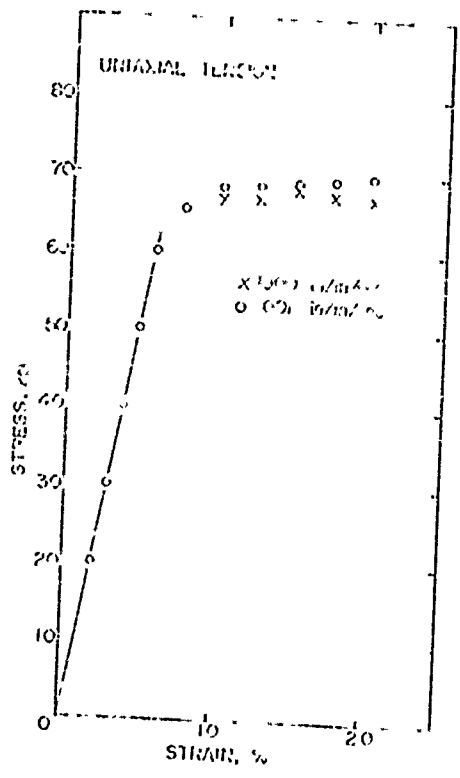

Figure 21. Stress-Strain for High Rate Uniaxial Tension

5 percent for the 0.5" gage length specimens aligned in the rolling direction. The corresponding reduction in area:

$$RA = \frac{A_o - A_f}{A_o}$$

where:

A_f = final area

A_o = initial area

ranged from 12 to 18 percent. (It should be pointed out that most of this scatter arises from measurement difficulties rather than material scatter, i.e., 0.001 inch diameter change equals ~ 2 percent reduction in area). In addition, axial elongation and reduction in area were found to be the same for tests conducted through the width of the plates. Through the thickness of the plate, however, a condition of anisotropic ductility exists. The axial elongation measured after fracture through the thickness was found to be a factor of 2 lower than the rolling and width orientation. This condition is shown schematically in Figure 22.

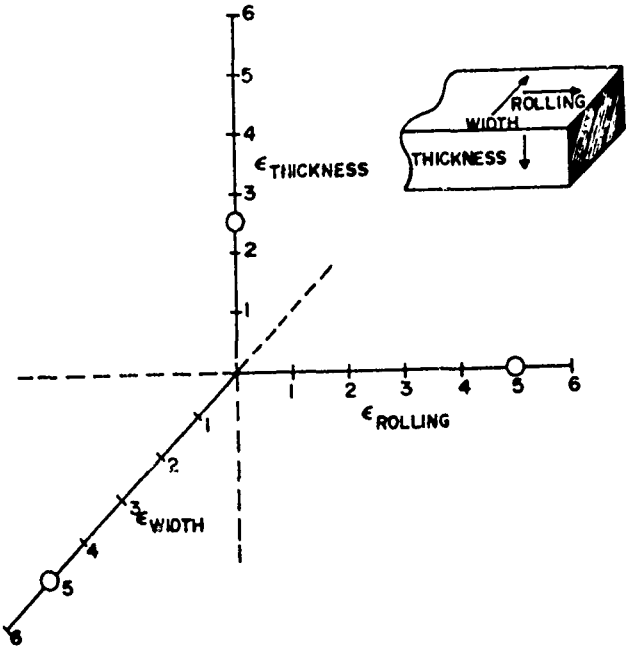

Figure 22. Axial Elongation to Failure in Three Plate Directions

Biaxial Tests

Table III lists the biaxial tests performed and the loading conditions. The majority of tests were conducted at an effective strain rate of approximately 10^{-4} sec^{-1} with a few added tests at a higher rate, approximately 1 sec^{-1}.

Before discussing the experimental results some definition of yield must be made. The definition used here is based on the square root of the second invariant of the stress deviator, $\sqrt{J_2'}$, (i.e., von Mises yield condition) plotted against the square root of the second invariant of the strain deviator, $\sqrt{I_2'}$, where:

$$\sqrt{J'_2} = \frac{1}{\sqrt{6}} \left[(\sigma_3 - \sigma_2)^2 + (\sigma_3 - \sigma_1)^2 + (\sigma_1 - \sigma_2)^2 + 6\tau_{12}^2\right]^{\frac{1}{2}}$$

$$\sqrt{I'_2} = \frac{1}{\sqrt{6}} \left[(\varepsilon_3 - \varepsilon_2)^2 + (\varepsilon_3 - \varepsilon_1)^2 + (\varepsilon_1 - \varepsilon_2)^2 + 6\psi_{12}^2\right]^{\frac{1}{2}}$$

where σ_1, σ_2, σ_3, τ_{12} and ε_1, ε_2, ε_3, ψ_{12} are the stresses and strains respectively with subscripts $_1$, $_2$, $_3$ referring to the axial, hoop and radial directions. ε_1 and ε_2 are generally measured strain gage values at the surface of the tube. ε_3, the strain through the wall of the tube, is readily calculated using elasticity equations during elastic loading and from the assumption of incompressible flow for the plastic components of strain (i.e., $\varepsilon_1^p + \varepsilon_2^p + \varepsilon_3^p = 0$) after yield. Deviatoric stress-strain curves for various tests are shown in Figure 23. Yielding is defined as the intercept of a line drawn parallel to the initial straight line portion of the curve at 0.2% strain off-set. For the cases where internal pressure was applied failure occurred before the 0.2% off-set. In these cases yield was defined as the highest stresses reached during the test.

TABLE III

BIAXIAL STRESS TESTS PERFORMED

TEST NUMBER	TEST TYPE (stress ratio)
1 & 2 (high rate)	Axial tension
3	Axial tension-- Internal pressure (1 to ½)
4	Axial tension-- Internal pressure (1 to 1)
5 & 6 (high rate)	Axial tension-- Internal pressure (½ to 1)
7 & 8 (high rate)	Internal pressure
9	Internal pressure Axial compression (1 to ½)
10	Internal pressure- Axial compression (1 to 1)
11 & 12 (high rate)	Pure torsion
13	Torsion- Axial compression (½ to 1)
14 & 15 (high rate)	Axial compression
16	External compression Axial tension (1 to 1)
17	Torsion-Axial tension (½ to 1)

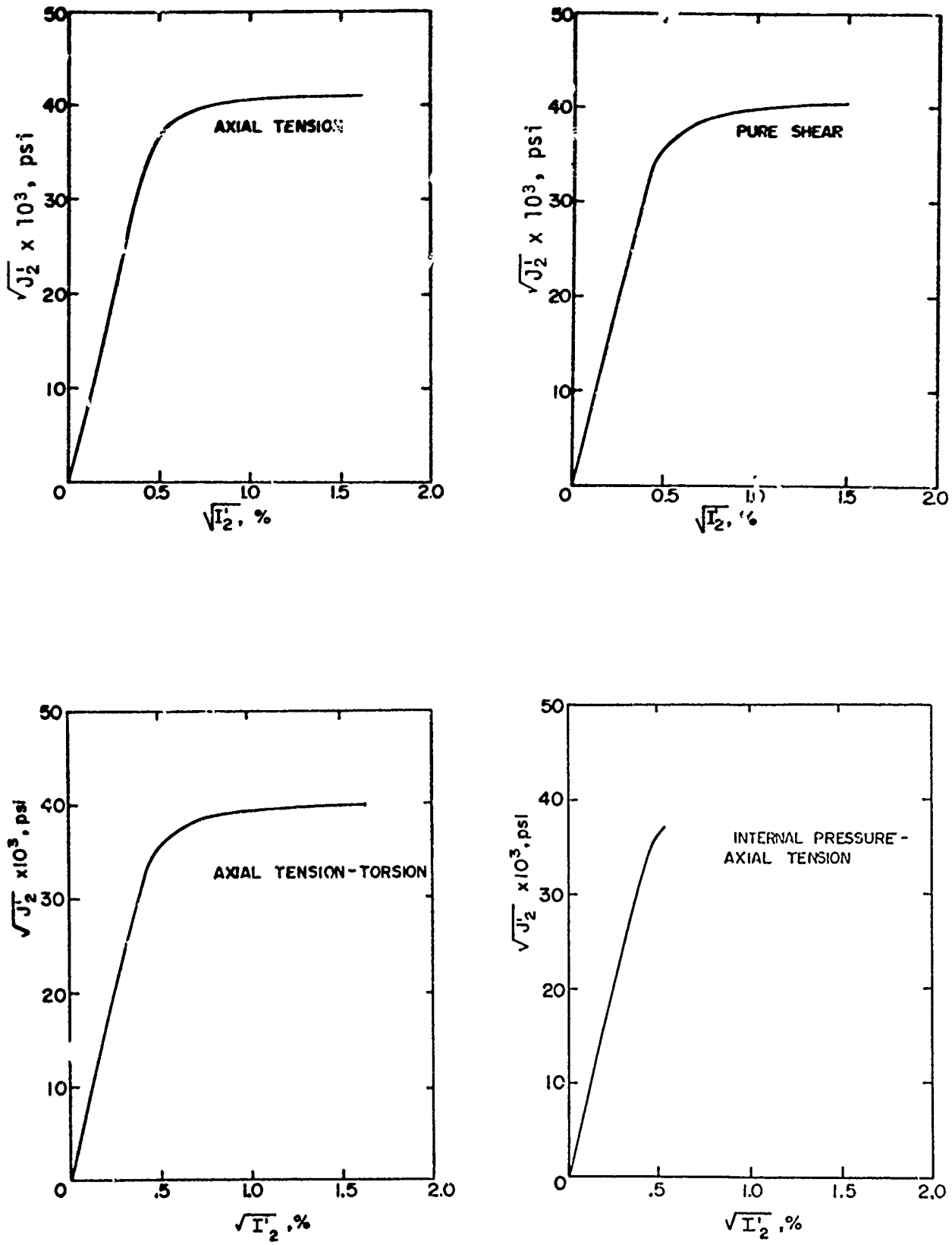

Figure 23. Deviatoric stress-strain curves for 2014-T651 aluminum tested under various loads.

For the series of tests presented here the strain rate was controlled to be constant on one axis while the second axis was controlled to provide a constant stress ratio (i.e., maintain proportional loading). Selection as to which axis would be maintained at constant strain rate was usually determined by the dominating stress. For example, referring to Table III, Test 5, it can be seen that the internal pressure is the major stress; therefore, the strain rate in the hoop direction was maintained constant. This procedure proved to work well with the calculated effective strain rate remaining relatively constant throughout the test while maintaining a constant stress ratio. Figure 24 shows the stress-strain time history for Test 5. As can be seen from the plot the three strains maintain approximately constant strain rates during elastic loading. When yielding first occurs a deviation in strain rate and stress ratio is noted. The effective plastic strain rate ($\dot{\varepsilon}_{eff}$) in this case was $\sim 2.9 \times 10^{-3}$ sec^{-1} where:

$$\dot{\varepsilon}_{eff} = \frac{1}{\sqrt{6}} \left[(\dot{\varepsilon}_3 - \dot{\varepsilon}_2)^2 + (\dot{\varepsilon}_3 - \dot{\varepsilon}_1)^2 + (\dot{\varepsilon}_1 - \dot{\varepsilon}_2)^2 + 6\dot{\psi}_{12}^2\right]^{\frac{1}{2}}$$

Yield

The yield surface under biaxial load is shown in Figure 25 in the Pi-plane for aluminum alloy 2014-T651 at different strain rates. Since agreement between the higher rate (~ 1 sec^{-1}) and slower rate ($\sim 10^{-4}$ sec^{-1}) was excellent (yield at 67 ± 2 KSI) we can conclude that the material is strain rate independent. Figure 25 indicates also that the material agrees reasonably well with the von Mises yield criteria - a circle in the Pi-plane for isotropic materials - except for the tension-tension quadrant.

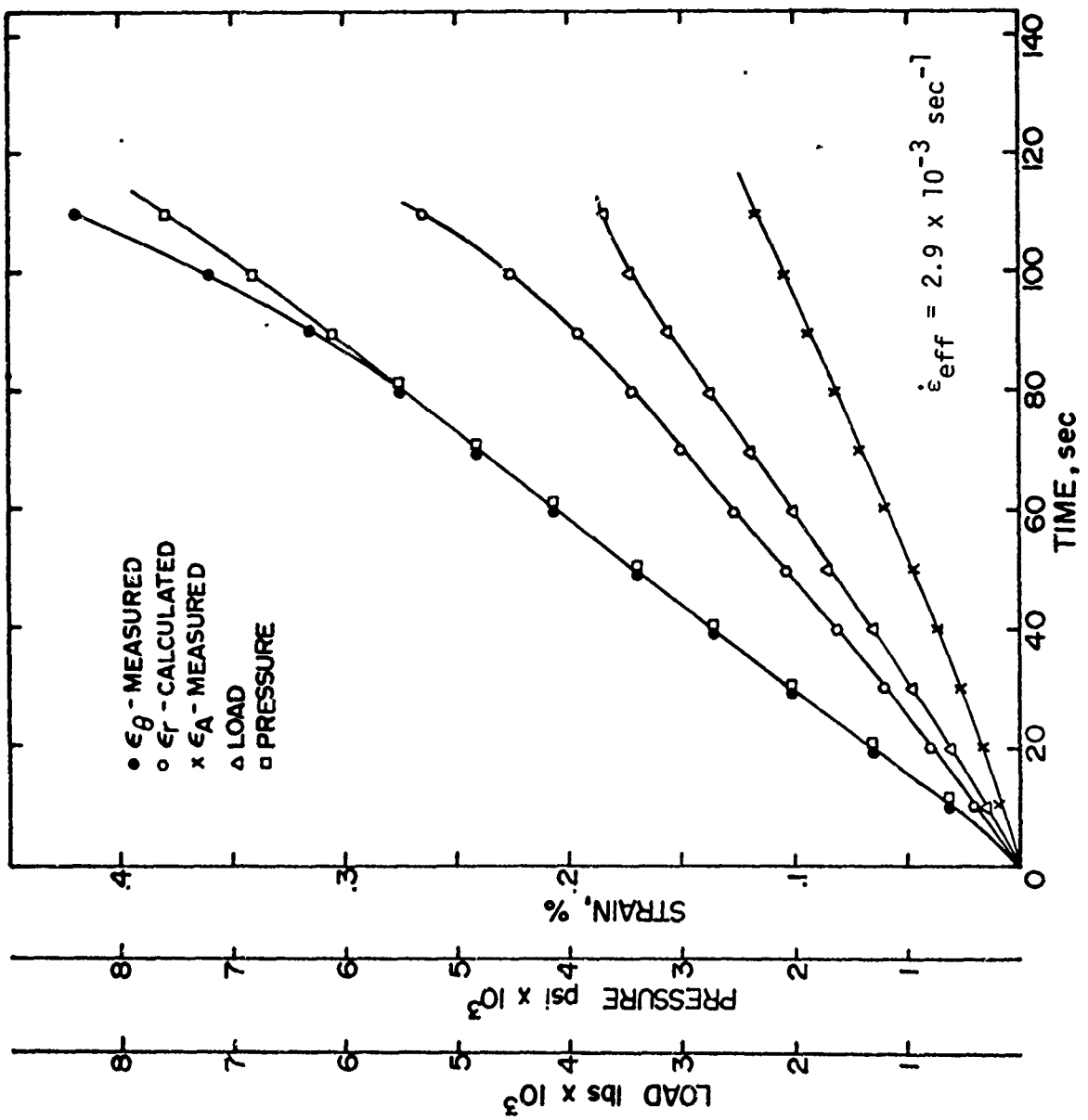

Figure 24. Typical Stress-Strain-Time History for Biaxial Test.

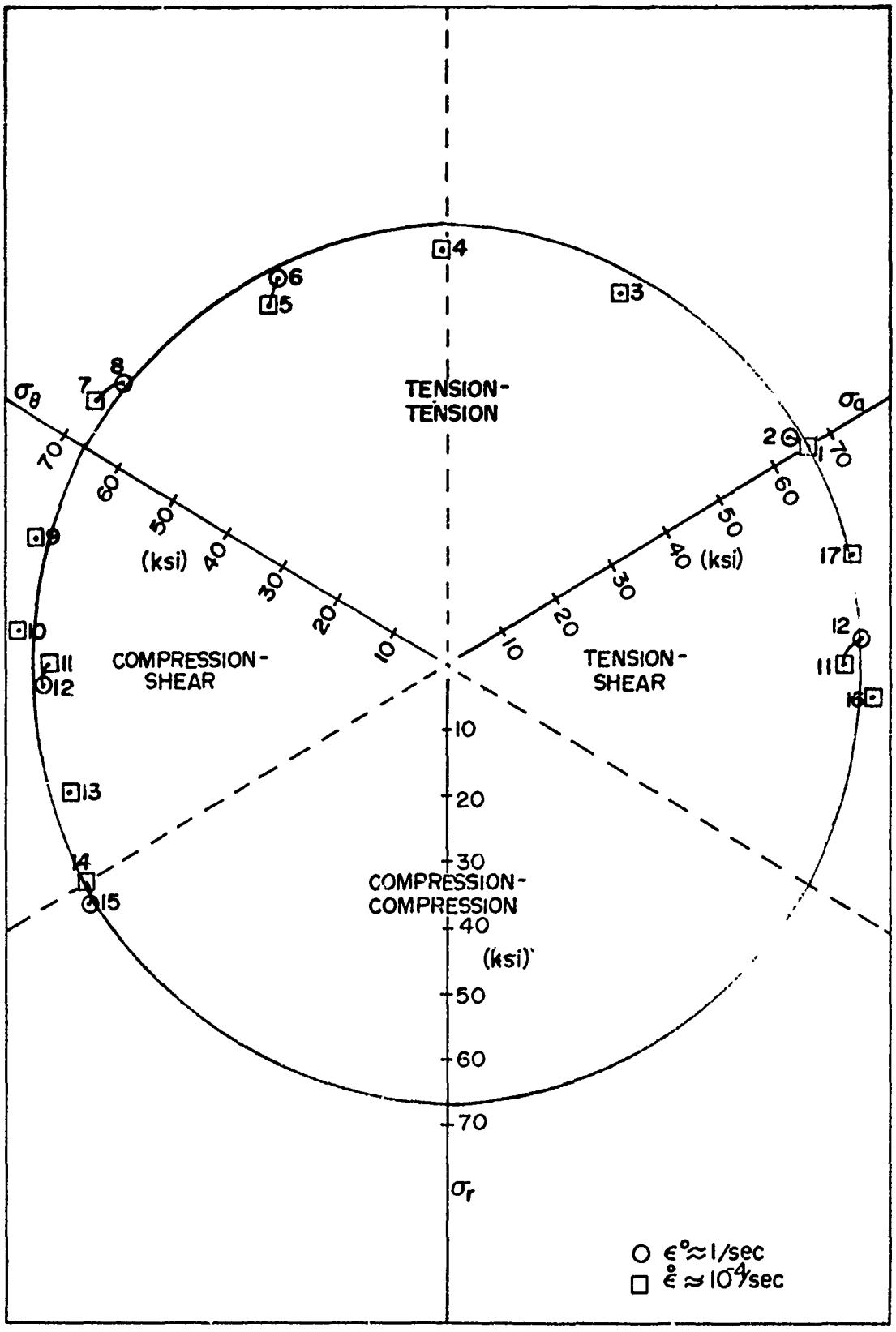

Figure 25. Yield surface for 2014-T651 aluminum alloy.
(Higher rates fall on top of slower rates)

Axial tension data observed with tubular specimens are seen to agree very well with test results for uniaxial tension specimens discussed earlier. Similar agreement was observed for pure compression. However, buckling (Figure 28a) was very evident with the axially compressed tubes at high strains in the post-yield region (6). Note that the tubular specimens shown in Figure 9 on being subjected to external pressure sense axial tension, σ_A, where

$$\sigma_A = \frac{A_1}{A_o} P_o = \frac{(r_1^2 - r_2^2)}{(r_2^3 - r_3^2)} P_o$$

where A_o = tube area, A_1 = area due to difference between r_1 and r_2, radii of the tube at the grip and gage sections respectively. The data point, Test #16, is seen to lie on the von Mises yield surface. Combined torsion/axial load yield stresses agree well with the von Mises yield surface. In pure torsion a negative axial strain occurred, on the order of .06 percent at failure. The axial shortening, however, is small compared to the shear strain induced by torsion.

Analysis of tests performed in the tension-tension quadrant indicated that the radial component of stress induced by the internal pressure was too large to be neglected ($\sim$ 10% of yield). It was therefore decided to calculate the stresses of the inside wall of the tubular specimen using thick-walled cylinder analysis as opposed to the more conventional thin-walled analysis, i.e.

$$\sigma_{\substack{\text{hoop} \\ (r=r_i)}} = P_i \frac{(r_o^2 + r_i^2)}{(r_o^2 - r_i^2)} \neq \frac{P_i r}{t}$$

$$\sigma_{\text{radial}} = - P_i \neq 0$$

where P_i = internal pressure, r = radius and t = thickness. This procedure accounts for all stresses present and, therefore, more accurately describes the yield stress state. The effect of neglecting the radial stress can best be seen in a two dimensional stress plot, Figure 26. This plot is simply the projection of Figure 25 onto a two dimensional plane (von Mises surface becomes an elipse with the equation $\sigma_A^2 - \sigma_A\sigma_\phi + \sigma_\phi^2 = K^2$, with K = 67,000 psi for this material) with test numbers corresponding to Table III. The dashed line in the tension-tension quadrant connects test points (X) analyzed using the thin-walled cylinder formula (Pr/t); "squashing" of the von Mises elipse is very pronounced. Thick-walled cylinder analysis, shown as circled data points, are seen to "extend" the yield surface but they still lie within the ellipse. The reason for the low yield in this region is the limited plastic flow exhibited prior to fracture, which occurred below the 0.2% off-set definition for yield.

Ductility

As indicated above, tests conducted in the tension-tension quadrant exhibit very little plastic strain with fracture occurring well below the 0.2% off-set definition of yield. This is not unusual (8, 9, 10) since this biaxial stress quadrant is much more sensitive to any material anisotropy or pre-working than any of the other quadrants. Indeed, it is the low ductility through plate thickness that dominates these results. This fact can be seen more clearly if the principal strains, ε_{axial} and ε_{hoop}, are plotted in a two dimensional plane as in Figure 27. This plot shows the uniform strain at fracture for specimens subjected to various stress states (data point numbers correspond to Table III). For this case "uniform strain" is defined as the strain that occurs in the area which is unaffected by any

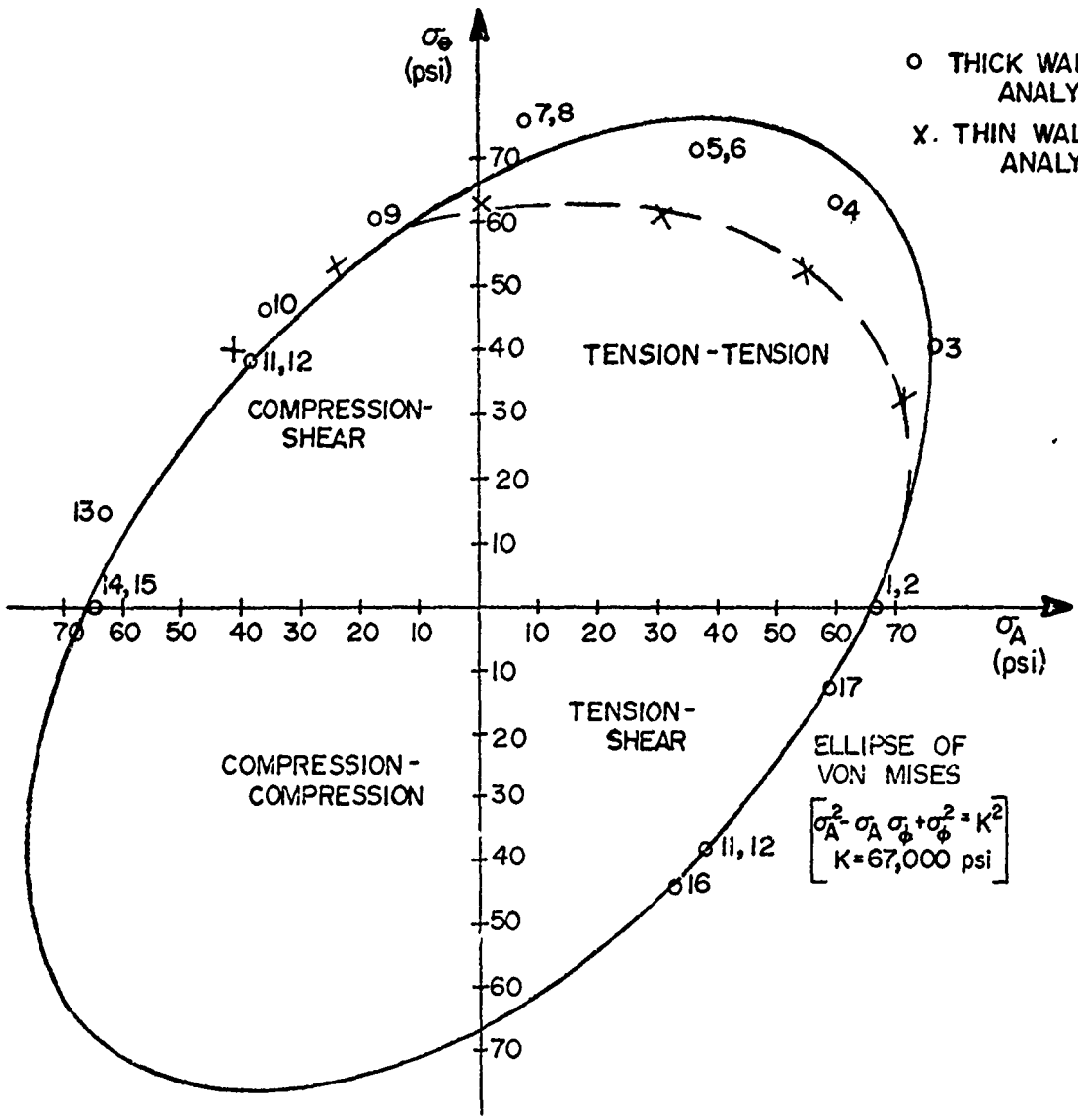

Figure 26. Two-Dimensional Yield Surface for 2014-T651 Aluminum Alloy.

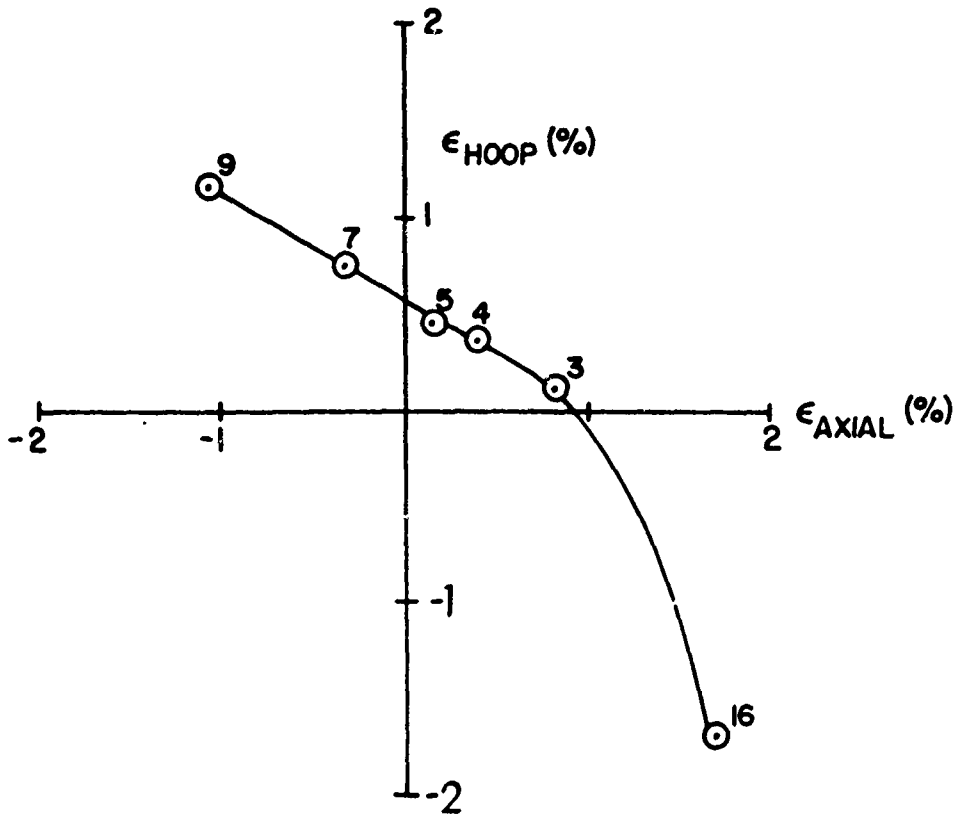

Figure 27. Uniform strain at fracture for biaxial tests.

localized necking associated with fracture. The low ductility exhibited in the tension-tension quadrant is dominated by the anisotropic behavior through the plate thickness. Figure 28d shows such a tensile failure. The failure surface is irregular and shows little plastic strain.

Figures 28c and e illustrate shear failures, the former as a result of torsional loading and the latter as a result of axial tension and external pressure. The shear failure again responded to the low ductility through the thickness with the failure resembling the irregular tensile failure.

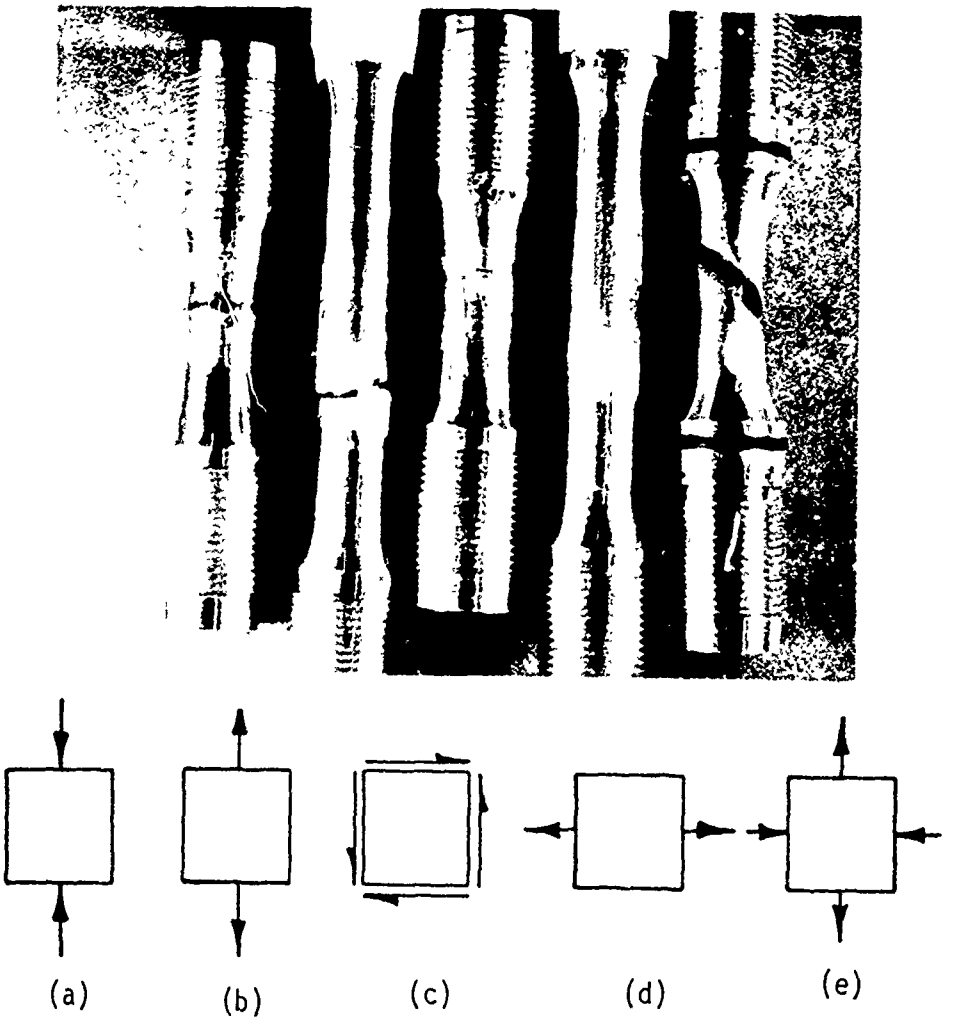

Figure 28. Biaxially Fractured Tubes

Fracture Toughness

Plane strain fracture toughness, K_{IC}, of 2014-T651 aluminum was determined according to ASTM E 399-72. Results of these tests performed at two different loading rates ($\sim$ 16 and 160 lb/sec), are shown in Table IV. As can be seen from the table, values of fracture toughness range from 23.5 to 25.6 ksi - $in^{\frac{1}{2}}$ (24.4 ksi - $in^{\frac{1}{2}}$ average) with no significant differences in results for the two rates performed. All tests were conducted at room temperature with

TABLE IV.

FRACTURE TOUGHNESS RESULTS FOR 2014-T651 ALUMINUM ALLOY
IN THE ROLLING DIRECTION

Specimen #	Specimen Description	Initial Fatigue Load A ∿ Max lbs B ∿ Min lbs	Fatique Cycles	Average Fatigue Crack Length (Ins)	Loading Rate (lb/sec)	K_{IC} ksi - $in^{\frac{1}{2}}$
2	Straight Cut	A = 990 B = 110	26,000	0.085	16	24.3
5	Chevron	A = 1010 B = 100	72,000	0.077	17	25.6
6	Chevron	A = 1000 B = 100	76,000	0.107	16	23.5
7	Chevron	A = 1000 B = 100	64,000	0.098	154	25.1
9	Chevron	A = 1100 B = 150	57,500	0.113	154	25.5
10	Chevron	A = 1020 B = 100	98,000	0.071	166	23.7
		K_{IC} = 24.4 ± 1.1 ksi - $in^{\frac{1}{2}}$				

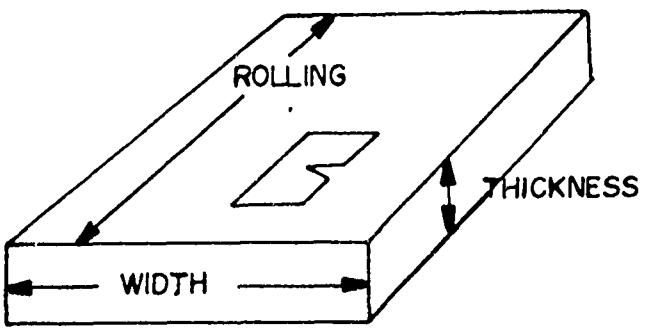

Figure 29. Fracture Toughness Specimen Orientation.

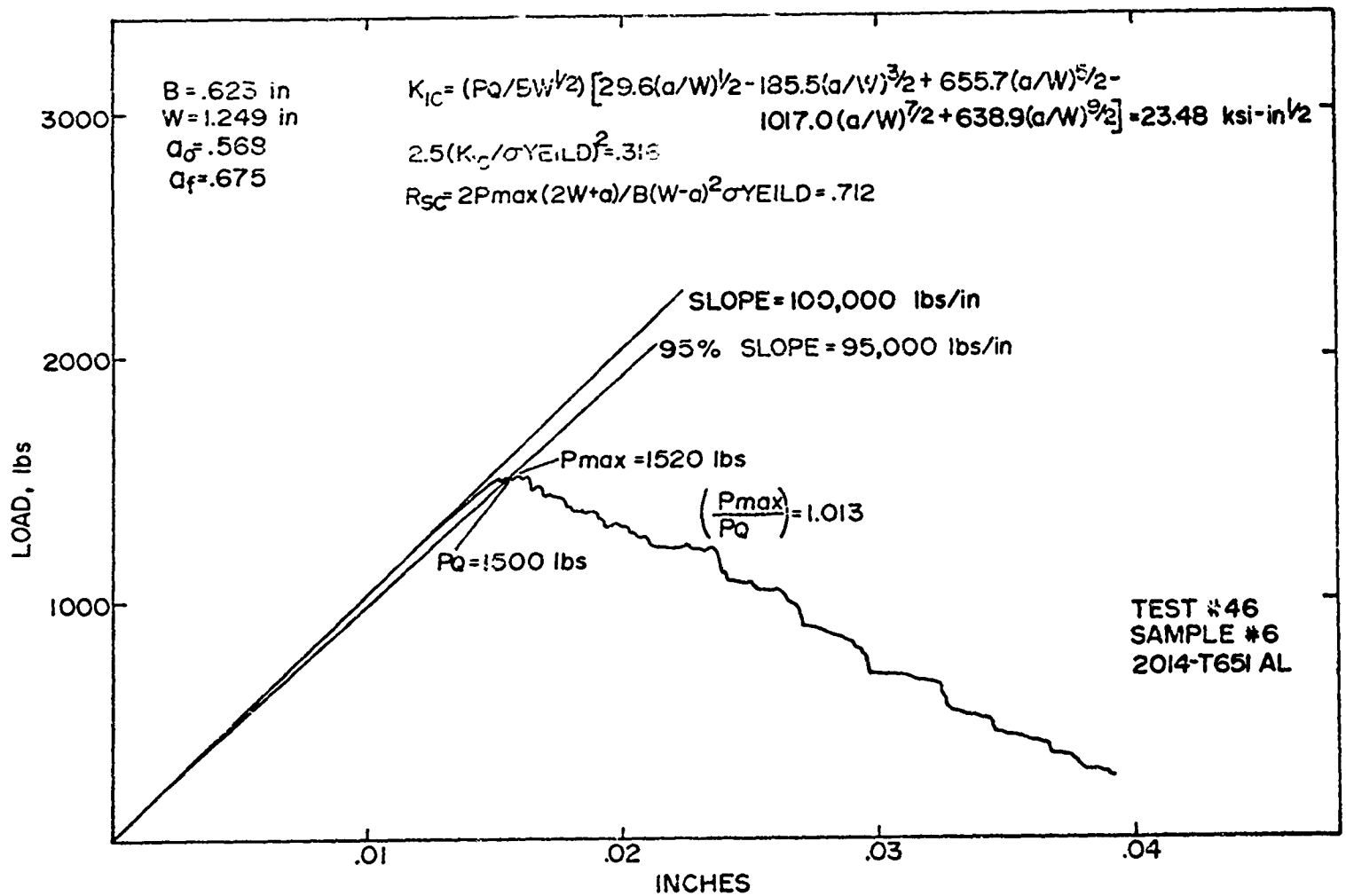

Figure 30. Typical Fracture Toughness Test Record.

the specimen orientation shown in Figure 29 (longitudinal-transverse specimens according to ASTM E 399-72).

Figure 30 shows a typical test record and appropriate calculations for a fracture toughness test. The figure shows the test to be valid according to Section 9.1.5 and 9.1.2 of ASTM E 399-72 (i.e., 2.5 $(K_{IC}/\sigma_{yield})^2$ is less than both the thickness and the crack length of the specimen and $P_{max}/P_Q < 1.1$ where P_{max} = maximum load sustained and P_Q = load at the intercept of a line with 95% of the slope of the initial straight line portion of the curve, see Figure 30) The specimen strength ratio, R_{sc}, ($R_{sc} = 2\ P_{max}(2w+a)/B(w-a)^2\ \sigma_{yield}$) is calculated to be 0.712 for this particular test. This value, however, appears to be representative for all tests performed here.

All fractures for the material were of the "fraction oblique" type (see ASTM E 399-72) with typical values of oblique fracture per unit thickness, (B-f)/B of 0.1 to 0.3. The fracture appearance of the material is seen in Figure 31. The extent of the fatigue crack is delineated by the fine textured fracture surface with the rest of the fracture having a coarser appearance.

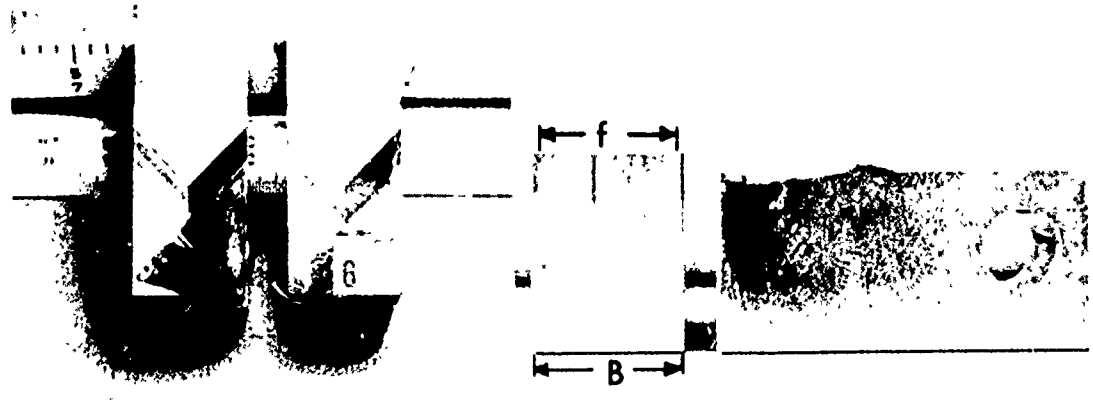

Figure 31. Failure Surface for Fracture Toughness Specimen.

Pin Bearing Strength

Pin type bearing strength tests were performed on the 2014-T651 aluminum alloy for two edge distance ratios and three thicknesses. Tests were performed in accordance with ASTM E-238 with the results shown in Table V.

TABLE V.

Pin Bearing Strength Results for 2014-T651 Aluminum Alloy in the Rolling Direction

Specimen #	Pin Diameter (in)	Edge Distance (in)	Edge Distance Ratio (approx.)	Plate Thickness (in)	Bearing Yield (ksi)	Bearing Strength (ksi)
0	0.2503	0.501	2	0.152	109.2	152.6
6	0.2503	0.501	2	0.1252	106.9	140.4
1	0.2503	0.501	2	0.103	109.1	147.6
5	0.2503	0.375	1.5	0.150	98.5	109.2
3	0.2503	0.375	1.5	0.1226	94.6	102.8
2	0.2503	0.375	1.5	0.095	98.9	109.5

When discussing the bearing strength of a material a few key definitions* are very beneficial:

bearing area -- the product of the pin diameter and specimen thickness.

bearing stress -- the force per unit of bearing area.

bearing strain -- the ratio of the bearing deformation of the bearing hole, in the direction of the applied force to the pin diameter.

---

* taken from ASTM E-238

bearing yield strength -- the bearing stress at which a material exhibits a specified limiting deviation from the proportionality of bearing stress to bearing strain.

bearing strength -- the maximum bearing stress which a material is capable of sustaining.

edge distance -- the distance from the edge of a bearing specimen to the center of the hole in the direction of applied force.

edge distance ratio -- the ratio of the edge distance to the pin diameter.

All tests were conducted at room temperature at a rate of approximately 0.1% bearing strain per minute on nominally 3.0" wide specimens.

A typical test record is seen in Figure 34. Bearing yield is calculated at an offset from the initial straight line portion of the record equal to 2% of the pin diameter. Bearing strength is simply the maximum load taken by the sample divided by the bearing area. Table V shows that an average bearing yield of 108.4 KSI was achieved for an edge distance ratio of 2 as opposed to an average of 97.3 KSI for the 1.5 edge distance ratio. The bearing strength for the large edge distance ratio was also higher, 146.8 KSI as compared to 107.2 KSI, for the smaller edge distance ratio. Note that bearing area, i.e., thickness of the plate used, has no effect on bearing yield or bearing strength.

The fracture, as seen in Figure 33 exhibits shear failure.

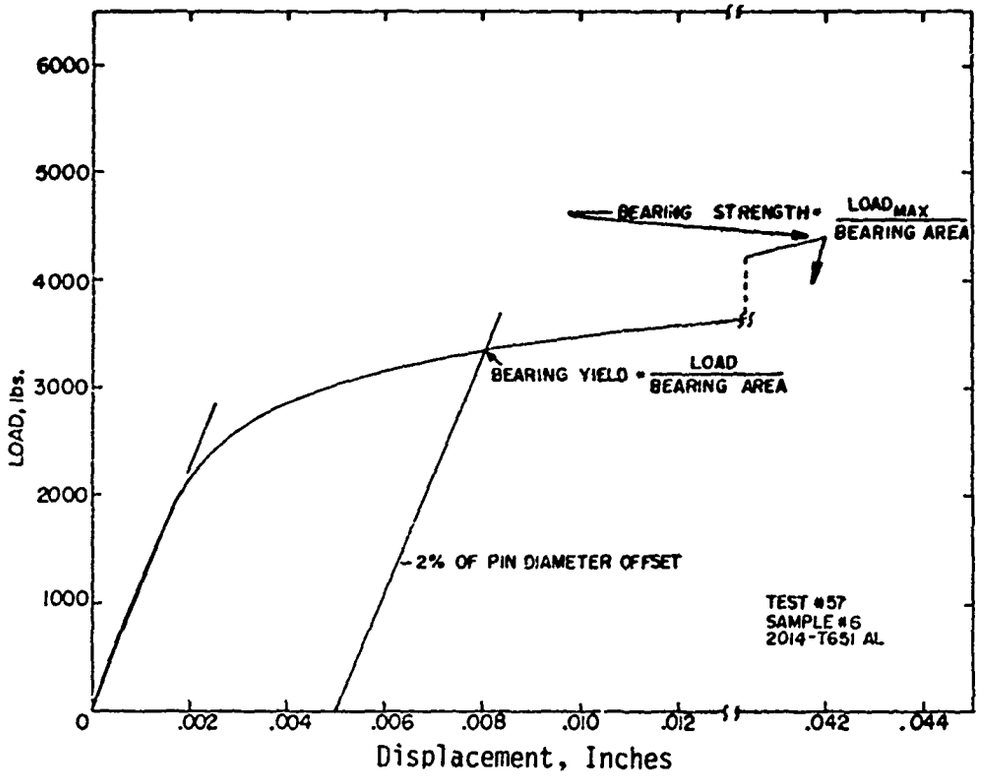

Figure 32. Typical Test Record for Pin Bearing Strength Test.

Figure 33. Failure for Pin Bearing Strength Specimen.

CONCLUSIONS

The series of tests performed show that 2014-T651 aluminum alloy is strain rate independent over the range tested (10^{-5} to 10^{3} sec^{-1}). Tests performed at various orientations within the plate indicate that a case of "anisotropic ductility" exists with minimum ductility through the thickness. The ductility through the thickness is a factor of two lower than either the rolling or width directions while yield is isotropic.

The effect of multiaxial stress of the material is seen to follow the von Mises yield criteria very well; at yield the square root of the second invariant of the deviatoric stresses is constant. The low ductility through the thickness, however, completely dominates the failure in the tension-tension stress quadrant. Whenever the sample is subjected to a tensile stress acting in the thickness direction, the sample failure occurs through this low ductility region. The material exhibits very little work hardening in tension, in constrast to the behavior in compression.

Fracture toughness values are also found to be independent of rate. The pin bearing strength of the material does not depend on the plate thickness. It does, however, depend on the edge distance ratio, increasing with increasing edge distance ratio.

REFERENCES

1. S. J. Green, J. D. Leasia, R. D. Perkins, and C. J. Maiden, "Development of Multiaxial Stress High Strain-Rate Techniques," Final Report Material Response Studies, SAMSO TR-68-71, Vol. III, MSL-68-8 Vol. III, January 1968.

2. K. D. Robertson, S. C. Chou, and J. H. Rainey, "Design and Operating Characteristics of a Split Hopkinson Pressure Bar Apparatus," Army Materials and Mechanics Research Center, AMMRC TR-71-49, November 1971.

3. C. J. Maiden and S. J. Green, "Response of Materials and Structures to Suddenly Applied Stress Loads," Interim Report Phase I, GM Defense Research Lab, DASA 1716, July 1965.

4. P. Mattaboni and E. Schreiber, *Journal of Geophysical Research, 72,* p. 5160, 1965.

5. S. G. Babcock, et. al., "Characterization of Three Aluminum Alloys," Final Report DAAG 46-69-C-0127, January 1971.

6. N. J. Hoff and T. Soong, "Buckling of Circular Cylindrical Shells in Axial Compression," *International Journal of Mechanical Science, Vol. 7, No. 7,* p. 489-520, July 1965.

7. U. S. Lindholm and L. M. Yeakley, "Effect of Strain Rate, Temperature and Multiaxial Stress on the Strength and Ductility of S-200E Beryllium and 6Al-4U Titanium," Southwest Research Institute, AFML-TR-71-37, March 1971.

8. B. H. Jones, "Assessing Instability of Thin-Walled Tubes Under Biaxial Stresses in the Plastic Range," *Exp. Mech., Vol. 8,* January 1968.

9. L. H. Sobel, "Effects of Boundary Conditions on the Stability of Cylinders Subject to Lateral and Axial Pressures," *AIAA Journal, Vol. 8, No. 8,* p. 1437-1440, 1964.

10. B. H. Jones and P. B. Mellor, "Plastic Flow and Instability Behavior of Thin-Walled Cylinders Subjected to Constant-Ratio Tensile Stress," *J. of Strain Analysis, Vol. 2, No. 1,* 1967.

11. R. Hill, *The Mathematical Theory of Plasticity,* Oxford University Press, London, England, 1960.

12. F. A. McClintock and A. S. Argon, *Mechanical Behavior of Materials,* Addison-Wesley Publishing Company, Inc., Reading, Massachusetts, 1966

ACKNOWLEDGEMENT

This report was prepared by Terra Tek, Inc., for the U. S. Army Materials and Mechanics Research Center, Watertown, Massachusetts, under Contract DAAG 46-74-C-0019. This work is part of the AMMRC program on Development of Hardened ABM Materials, Mr. J. F. Dignam, Program Manager. The AMMRC Technical Supervisor was Dr. S. C. Chou.

The authors wish to extend their appreciation to Dr. S. C. Chou and Mr. J. F. Dignam of the U. S. Army Materials and Mechanics Research Center for the technical contributions and support provided throughout the project. Also Mr. R. M. Griffin and Mr. J. M. Brammer are acknowledged for their design work on the test machine, Mr. A. W. Rae for his assistance during the project, Ms. Beth Zimmerman and Ms. Dawn Hansen for the artwork and Ms. Carole Marlor for the preparation of the manuscript.